1	Gravel liquefaction assessment using dynamic cone penetration and shear wave velocity
2	tests based on field performance from the 1964 Alaska earthquake
3	Jashod Roy ¹ , Kyle M. Rollins ² , Adda Athanasopoulos-Zekkos ³ , McKay Harper ⁴ , Nicolas
4	Linton ⁵ , Michelle Basham ⁶ , William Greenwood ⁷ , Dimitrios Zekkos ⁸
5 6 7	¹ Research Asst., Civil & Environ. Engrg. Dept., Brigham Young Univ, 430 Engineering Bldg., Provo, UT 84602, ORCID: https://orcid.org/0000-0003-0854-3790 , email: jashod.roy@gmail.com
8 9	² Prof., Civil and Environ. Engrg. Dept., Brigham Young Univ., 430 Engineering Bldg., Provo, UT 84602, ORCID: https://orcid.org/0000-0002-8977-6619 , email: rollinsk@byu.edu
10 11	³ Assoc. Prof., Civil & Environ. Engrg. Dept., Univ. of California, Berkeley, Berkeley, CA, ORCID: https://orcid.org/0000-0002-3785-9009 , email: adda.zekkos@berkeley.edu
12 13 14	⁴ Staff Engineer, RB&G Engineering, Inc., 820 N. 1435 W., Provo, UT 84604, email: mckayharper@gmail.com
15 16 17	⁵ Research Assistant, Civil & Environ. Engrg. Dept., Brigham Young Univ, 430 Engineering Bldg., Provo, UT 84602, email: nlinton24@gmail.com
18 19 20	⁶ Research Assistant, Civil Engrg. Dept., Univ. of Michigan, Ann Arbor, MI, ORCID: https://orcid.org/0000-0002-0184-6097 , email: mbasham@umich.edu
21 22	⁷ Program Manager, Mathworks, Natick, MA,
23242526	⁸ Assoc. Prof., Civil & Environ. Engrg. Dept., Univ. of California, Berkeley, Berkeley, CA, ORCID: https://orcid.org/0000-0001-9907-3362 , email: zekkos@berkeley.edu
27 28	Corresponding author email: jashod.roy@gmail.com
29	
30	
31	
32	
33	

ABSTRACT

34

35

36

37

38

39

40

41

42

43

44

45

46

47

48

49

50

Evaluating the liquefaction potential of gravelly soils using in-situ testing remains a challenge in geotechnical engineering practice. The Chinese Dynamic Cone Penetration (DPT) test provides an alternative for in-situ testing in gravelly soils to Becker Penetration Test (BPT) and the Standard Penetration test (SPT). The Chinese DPT was recently correlated with liquefaction resistance based on field performance data from the M_w 7.9 Wenchuan earthquake. In this study, liquefaction resistance was evaluated using the DPT and shear wave velocity measurements at eight sites in Seward and Old Valdez, Alaska, where gravel liquefaction took place and two sites in Valdez, where no liquefaction occurred in the 1964 Alaska earthquake. The DPT-based liquefaction triggering curve predicted liquefaction potential at all test sites with moderate accuracy. N'120 blow counts from SPT hammers were generally consistent with those from the DPT hammer after energy correction. Back-calculated energy correction factors were typically within 10% of the theoretical energy correction factor. These results suggest that the DPT can provide liquefaction hazard evaluations accurately and economically for many gravelly soils. Liquefaction evaluations using currently available V_s -based triggering curves developed for sands often indicated no liquefaction at sites where liquefaction occurred at the Alaska sites. In contrast, a V_s-based triggering curve developed from a data set of gravelly soil sites correctly predicted liquefaction at all sites.

52

51

- Author keywords: Gravel, Liquefaction, Dynamic Cone Penetrometer (DPT), shear wave
- velocity, Alaska Earthquake, MASW

55

1. INTRODUCTION

A significant number of gravel liquefaction case histories are known to have occurred during major earthquakes over the past 100 years e.g., 1964 Alaska earthquake [1,2], 1976 Friuli earthquake in Italy [3], 1985 Borah Peak earthquake in Idaho [4], 2008 Wenchuan earthquake at the Chengdu Plain in China [5], 2014 Cephalonia earthquakes in Greece [6], 2016 Kaikoura earthquake in New Zealand [7] and many more. Still, the characterization of gravelly soils and assessment of liquefaction hazards in a reliable, cost-effective manner has always been a challenging problem in geotechnical engineering practice. Therefore, improved field methods for characterizing and assessing the liquefaction potential of gravelly soil are sorely needed.

Among the in-situ testing methods, the standard penetration test (SPT) and cone penetration test (CPT) are not very suitable in gravelly soils, because of interference with large-size particles. Due to this interference, the SPT or CPT results can be deceptive as the penetration resistance may increase even when the soil is not particularly dense. Hence, it becomes very difficult to obtain a consistent and reliable correlation between SPT or CPT penetration resistance and fundamental gravelly soil properties, such as liquefaction resistance. To overcome this limitation, the Becker Penetration Test (BPT) has become the primary field test used to evaluate liquefaction resistance of gravelly soils in North American practice [8]. The BPT is performed by hammering a closedend 168-mm diameter casing into the ground. The large diameter of the BPT is intended to reduce the effect of particle size on the penetration resistance. However, this test is not available in most locations throughout the world, is expensive and has significant uncertainty because the liquefaction resistance is determined from an SPT blow count derived from a correlation with the BPT blow count. In addition, corrections for shaft friction and chamber pressure [9] are needed. Although innovative instrumentation approaches, such as the iBPT promise to provide more

accurate estimates of the energy actually delivered to the toe of the BPT [9], these efforts do not reduce the cost and complexity of the test procedure.

80

81

82

83

84

85

86

87

88

89

90

91

92

93

94

95

96

97

98

99

100

101

102

As an alternative in-situ test in gravelly soils, the penetration resistance from a dynamic cone penetration test (DPT) developed in China has been correlated with liquefaction resistance based on field performance data from the M_w 7.9 Wenchuan earthquake [5]. The Chinese DPT consists of a 74 mm diameter cone tip continuously driven by a 120 kg hammer with a free fall height of 100 cm using a 60 mm drill rod to reduce friction. At 74 mm, the DPT diameter is 50% larger than the SPT and 110% larger than a standard 10 cm² CPT; however, it is still 55% smaller than the BPT. Clearly, the BPT provides the largest diameter to particle size ratio of all the tests, which is a desirable attribute, but the DPT diameter is significantly larger than the SPT or CPT and could be a reasonable solution in many cases depending on percentage and size of gravel particles in the soil matrix. Andrus [10] reported that SPT-N values measured in the gravelly deposits at Pence Ranch and Whiskey Springs (60-70% Gravel Content) are 60% too high in comparison to the companion BPT testing. On the other hand, the recent investigation by Rollins et al. [3] at the gravelly sites in Avasinis, Italy (30-40% gravel content) showed that the SPT procedure quite successfully predicted the liquefaction potential of the loose gravelly deposits. Recent CPT investigations [7] at the gravelly reclamation land at Centerport in Wellington, New Zealand (gravel content around 60-70% with 30-40% larger than 10-15 mm) showed a considerable number of spikes in the CPT resistance profile due to interference with large particles. Hence, the DPT could be more useful over SPT/CPT for those gravelly deposits where gravel percentage is relatively higher (above 30-40% as per 2-4.75 mm particle size criterion), however the density of the soil deposit may also play a significant role in this aspect. As far as the effect of particle size is concerned, Meyerhof [11] stated that all penetration tests become unreliable if the maximum

particle size approaches the diameter of the penetrometer or the sampler spoon. Iqbal et al. [12] reported that the static CPT results begin to be affected when the particle size becomes greater than one-third of the cone diameter. Therefore, some artificial increase in the DPT blow count might be expected if the DPT cone encountered relatively large particles (higher than one third of the cone diameter) in dense soil deposits. However, further investigation is still required to bring specific quantification regarding the effect of particle size and percentage of gravel particles on the performance of DPT in characterizing gravelly sites.

103

104

105

106

107

108

109

110

111

112

113

114

115

116

117

118

119

120

121

122

123

124

125

Over the past 60 years, Chinese engineers have observed that the DPT is effective in penetrating coarse or cobbly gravels and provides penetration data useful for foundation design [13]. Following the 2008 M_w 7.9 Wenchuan earthquake in China, Cao et al. [5] conducted 47 DPT soundings at 19 sites with observed liquefaction effects and 28 nearby sites without liquefaction effects. Most of these sites consisted of 2 to 4 m of clayey soils, which were underlain by 500 m thick gravel beds containing 30-70% of gravel content [5]. DPT soundings reached depths as great as 20 m, readily penetrating gravelly layers that liquefied as well as deeper layers that were too dense to liquefy. DPT soundings were typically extended to 20 m or into a dense layer because it is unlikely to have a liquefiable layer greater than this depth that would produce liquefaction features at the ground surface [14, 15].". Using DPT data for the M_w 7.9 Wenchuan earthquake, Cao et al. [5] developed probabilistic liquefaction triggering curves based on the DPT blow count; however, the data set is rather limited and based on one earthquake. Thus, liquefaction resistance has been directly correlated with DPT blow count from field case histories eliminating the need to convert the DPT blow count to an equivalent SPT blow count and significantly reducing uncertainty in liquefaction assessment. Therefore, the DPT could provide an important new procedure for characterization of gravels and fill a gap in current geotechnical practice between

CPT/SPT and BPT testing. As per the existing literature, for the gravelly deposits having more than 20-30% of gravel content, this DPT-based liquefaction triggering procedure would be more useful than the existing sand-based SPT or CPT triggering procedures as the penetration resistance of these deposits may be significantly influenced by the gravel content.

As an alternative to penetration testing, some researchers have proposed liquefaction triggering curves based on the shear wave velocity, V_s . This method eliminates problems associated with particle size interference and can even be performed using surface wave methods that eliminate the need for a borehole. Andrus and Stokoe [16] and Kayen et al. [17] proposed liquefaction triggering curves for sands; however, a number or researchers have found that these methods predict no liquefaction at gravel sites where liquefaction was actually observed in earthquake case histories [3, 6, 18, 19]. Both Cao et al. [18] and Chang [19] developed V_s -based liquefaction triggering curves specifically based on gravel liquefaction case histories.

In this study, DPT soundings were performed at Seward and the port of Old Valdez in Alaska where gravel liquefaction occurred and at Valdez, Alaska, where gravel did not liquefy in the 1964 M_W 9.2 Alaska earthquake. In addition, V_s profiles were developed based on Multichannel Surface Wave (MASW) testing at the sites in Seward and Old Valdez. The site map showing the locations of Seward, Old Valdez and Valdez with respect to the epicenter of the Alaska earthquake are provided in Fig. 1. The data points obtained from these investigations are important because they are associated with the highest cyclic stress ratios (CSRs) in any liquefaction triggering database and the highest magnitude event. As a result, they will have a strong influence on the shape of future triggering curve for higher DPT blow counts and V_s values. The objectives of this study are: (1) to investigate the applicability of DPT and V_s -based liquefaction triggering methods to evaluate the liquefaction potential of gravelly soils, (2) to expand the database of DPT and V_s liquefaction

case histories in gravelly soils to facilitate the development of improved predictive models in the future, and (3) to evaluate the potential of using the SPT hammer energy in place of the heavier DPT hammer to evaluate liquefaction potential after standard correction procedures for hammer energy.

2. GEOLOGIC SETTING AND LIQUEFACTION EFFECTS

2.1. Port Valdez

The geologic setting at Port Valdez consists of one bedrock unit and three depositional complexes of unconsolidated sediments [1]. The bedrock has an interbedded structure with thick beds consisting of layers of argillite, arkosic sandstone and conglomerate as described by Moffit [20]. These rocks have well developed bedding striking east-west and dip towards the north. Repeated glacial erosion in the past produced these ice-scoured outcrops on the surface of the bedrock.

At the eastern end of the port, the deltaic complex formed by the coalescence of outwash plains of Mineral Creek on the north and the Valdez Glacier Stream, Robe River, Lowe River on the south is composed of a thick section of poorly consolidated silt, fine sand and gravel. The surficial beds of stream deposited glacial outwash gravel and have a gentle slope towards the south and southwest. The water table lies within a few meters of the surface indicating that nearly the entire section is fully saturated.

The Mineral Creek alluvial fan lying at the northwest side of Valdez consists of Holocene deposits [21] (https://www.mindat.org/loc-198893.html) which formed in an elongated depression between the main valley wall and a parallel outlying bedrock ridge. The fan has a slope height of approximately 18 m above mean sea level at the mountain front that slopes downward to sea level. Investigations conducted by Shannon and Wilson [22] for the US Army Corps of Engineers show

that this alluvial fan consists of more than 30 m of medium dense to very dense gravelly sand with some fraction of medium to coarse cobbles remaining in the soil matrix. Because of the high tidal range, broad tidal flats composed of silt, fine sand and organic muds are deposited near the surface at the seaward edge of the outwash delta and Mineral Creek.

Old Valdez lies just north of the glacial outwash fan produced by the Valdez Glacier Stream. Investigations conducted by the Alaska Dept. of Transportation (ADOT) indicate that the fan consists of more than 30 m of loose to medium dense sandy gravel and gravelly sand layers [1]. Fig. 2 shows the locations of the boreholes drilled by ADOT.

Due to strong earthquake shaking, large fissures were observed to open and close along the streets near the Old Valdez dock as the non-liquefied surface blocks oscillated on the underlying liquefied layers. Water saturated gravel with silt and sand was also observed erupting from many fissures, indicating liquefaction of gravelly soil [1]. Above all, the most disastrous incident caused by the earthquake was a submarine landslide at the Old Valdez port near the Mineral Creek side. When subjected to cyclic shear stresses, the contractive sandy gravel sediments developed excess pore pressures that produced liquefaction. When the shear strength of the liquefied sediment became less than the static gravitational shear stresses, a slide mass about 1500 m long with a volume of 4 x 10⁸ cubic meters slid into Prince William Sound [23, 24]. As shown in Fig. 2, the slide sliced off the ends of the two piers (shown with dashed lines) destroying the harbor facilities. The slope failure caused the death of about 30 people and created a new shoreline with a steep scarp [1].

Following the flow slide, the relatively flat slope (1.2%) behind the new shoreline experienced lateral spread displacements, as the land moved towards the free face created by the scarp. In this case, the residual shear strength of the sandy gravel after liquefaction was greater

than the gravitational static shear stresses acting on the slide mass, which prevented a flow slide. However, the combination of static and inertia forces acting on the mass during the earthquake shaking transiently exceeded the residual strength, allowing incremental downslope movements to accumulate [25]. Ultimately, measured seaward movements between 7th St. and McKinley St. (see Fig. 2) after the earthquake were between 3.1 and 5.0 m. These liquefaction-induced movements produced a series of ground fissures, shown by red lines on Fig. 2, generally oriented parallel to the new shoreline. The fissures caused severe disruption to buildings as well as to water and sewer pipelines [1].

In contrast, the area now known as Valdez, situated on the north side of the Valdez port, consists of denser deposits that did not show any sign of liquefaction ejecta or lateral spreading during the earthquake. Geotechnical investigations by Shannon and Wilson [22] for the US Army Corps of Engineers confirmed the presence of dense sandy gravels throughout this area. Therefore, the town of Valdez and the port facility was moved to this new location after the disaster took place in the old Valdez area.

2.2. Seward

Seward is situated on glacial outwash deposits sandwiched between the steep, glacier filled slopes of the Kenai Peninsula on the northwest and the ocean to the southeast. The glacial outwash was deposited by the Resurrection River that has a maximum recorded flow volume of 5660 m³/s capable of transporting coarse gravel and cobbles along with sand. During the 1964 Great Alaskan earthquake, the outwash flood plain surface became extensively fractured due to liquefaction-induced lateral spreading towards the river as shown in Fig. 3. Water saturated gravelly sand erupted from the fissures indicating that liquefaction had occurred in the gravelly soil deposit [2]. Consequent lateral spread displacement of the gravelly sediments caused significant damage to

three railroad and highway bridge structures crossing the Resurrection River and Mineral Creek [2]. Despite having pile foundations supporting the bridge abutments and piers, the ground behind these bridges moved about one meter towards the river, causing the bridges to be compressed and buckled as the bridge piers rotated towards the river [2]. In addition, a few piles were shifted downstream, and others suffered excessive downdrag settlement after liquefaction.

The location of the three bridges along the Resurrection River are shown in Fig. 3 along with the ground fissures and cracks caused by lateral spreading as shown by the black lines. Site investigation was performed by the Alaska DOT at several locations near the bridge abutments as shown by the black dots on Fig. 3. These investigations show that the soil deposits near the bridges in Seward generally consist of loose to medium dense sandy gravel with some silt content.

The range of grain size distribution curves for the test sites in Old Valdez, Valdez and Seward in Alaska based on the geotechnical reports are shown in Fig. 4. It is observed from the gradation curves that the gravel content varies from 15 to 65%, the sand content varies from 35-85% and the coefficient of uniformity (C_u) varies from 15 to 47. Detailed information on the average gradation curve for each site is given in Table 1. Detailed information on the average gradation curve for each site is given in Table 1. These gradation curves indicate that the soil deposits at all the investigation sites are composed of well graded gravelly soil. The D_{50} size varies from 2 to 12 mm for all sites which is less than 33% of the diameter of the DPT cone (74 mm). This indicates that gravel size particles are not likely to have any significant effect on the DPT penetration resistance [12]. In addition, because the sand content at these sites is greater than 30%, the hydraulic conductivity is likely to be controlled by the sand fraction [26] making the gravel susceptible to liquefaction even without an impervious surface layer.

3. DPT TESTING AND INTERPRETATION

241

242

243

244

245

246

247

248

249

250

251

252

253

254

255

256

257

258

259

260

261

262

263

As part of this study, DPT soundings were performed at 12 different locations (Site 1 near a bridge, Sites 2 through 6 near the port facilities of Old Valdez (liquefied during 1964 Alaska event) and Sites 7 and 8 in Valdez (no liquefaction took place) as well as four sites (Sites 9 through 12 near bridges where liquefaction occurred during 1964 Alaska event) in Seward as shown in Fig. 2 and 3, respectively. The DPT boreholes are close to the locations of the boreholes drilled by the Alaska Department of Transportation from which the generalized soil profiles were obtained.

In this study, the standard Chinese DPT consisting of a 74 mm cone tip attached with a 60 mm drill rod has been used. The tests were conducted using a CME drill rig with the capability of using two different hammer energies. At sites in Seward and three sites (Site 2, Site 4 and Site 5) at Old Valdez, the DPT sounding was initially performed using an automatic SPT hammer with a weight of 63.5 kg (140 lbs) dropped from a height of 0.76 m (30 in). Thereafter, a second sounding was performed about a meter away using a 154 kg (340 lbs) automatic hammer with a drop height of 0.76 m (30 in). This hammer weight-drop height combination produced a drop energy that is comparable to that of the standard Chinese DPT hammer. These tests were performed to evaluate the ability of the SPT hammer to produce blow counts comparable to those obtained with the standard Chinese DPT hammer after correction for hammer energy, as discussed subsequently. An SPT hammer energy could potentially provide more resolution in the blow count for loose gravels and would be more readily available to practicing engineers in the geotechnical engineering field. However, it should be noted that the DPT hammer energy per unit area is not equivalent to the energy per unit area for SPT although the DPT procedure seems to be similar to the SPT. The frictional energy loss is different in DPT and SPT as the DPT uses a much larger diameter cone compared to the SPT rod.

At the other locations near the Old Port and Valdez area, DPT tests were only performed using the heavy hammer energy. Hammer energy measurements were made using an instrumented rod section and a Pile Driving Analyzer (PDA) device from PDI, Inc. These energy measurements indicate that the 63.5 kg (140 lbs) and the 154 kg (340 lbs) hammers delivered averages of 94% and 95% of their theoretical free-fall energies, respectively.

Based on 1200 hammer energy measurements, Cao et al. [27] found that the Chinese DPT provided an average of 89% of the theoretical free-fall energy ($E_{Chinese\ DPT}$). Because the energy delivered by a given hammer (E_{Hammer}) may differ from the energy typically supplied by a Chinese DPT hammer ($E_{Chinese\ DPT}$), it may be necessary to correct the measured blow count. In this study, the hammer energy correction was made using the simple linear reduction suggested by Seed et al. [28] for SPT testing

$$N_{120} = N_{Hammer} (E_{Hammer}/E_{Chinese\ DPT}) \tag{1}$$

where N_{Hammer} is the number of blows per 0.3 m of penetration obtained with a hammer delivering an energy of E_{Hammer} . Here, the delivered hammer energy (E_{Hammer}) is actually the theoretical hammer energy times the hammer efficiency (94% and 95% for the light and heavy hammers, respectively). The mean ratio of hammer energy delivered, divided by the energy delivered by the Chinese DPT hammer was 1.04 and 0.42 for the 154 kg and 63.5 kg hammers, respectively.

The DPT blow count value, N_{120} , represents the number of hammer blows to drive the penetrometer 30 cm. Although, blow counts are recorded for every 10 cm penetration at the site, they are multiplied by three to calculate an equivalent N_{120} for 30 cm penetration, also preserving the detailed 10-cm readings in the penetration profile. The 30-cm drive length is specified to be consistent with the drive length of the SPT [5].

In addition, Cao et al. [5] recommended an overburden correction factor, C_n to obtain the normalized N'_{120} value using the equation

$$N'_{120} = N_{120} C_n \tag{2}$$

where

$$C_n = (100/\sigma'_{vo})^{0.5} \le 1.7 \tag{3}$$

and $\sigma'_{\nu\sigma}$ is the initial vertical effective stress in kN/m². A limiting value of 1.7 was added to be consistent with the C_n used to correct penetration resistance from other in-situ tests (Youd et al. 2001). Plots of the energy corrected DPT N'_{120} versus depth profiles are provided in Figs. 5 through 10 for sites in Old Valdez, Figs. 11 and 12 for sites in Valdez, and Fig. 13 through 16 for sites in Seward.

A comparison of the profiles obtained by two different hammer energies indicates that the agreement obtained with the simple energy correction factor in Eq. (1) is reasonably good in most cases. At Site 5 in Valdez and Site 12 at Seward, the N'_{120} for both hammers agree remarkably well. At sites 10 and 11 in Seward and Sites 2 and 4 in Valdez, the N'_{120} values for the light hammer appear to be higher below 10 m although reasonable agreement is observed above 10 m depth except some occasional discrepancies caused by the local variations in soil strata between two adjacent boreholes. At site 9 in Seward, the light hammer is consistently higher than the heavy hammer. This divergence at Site 9 in Seward is attributed to the fact that the light hammer did not penetrate vertically and likely developed higher friction on the drill rods, artificially increasing the blow counts. Although some amount of energy loss could occur due to friction along the DPT rod, it should still not affect the blow count substantially for the depth range of interest if the vertical insertion of the rod is maintained during penetration testing. Chinese experience indicates that friction is not substantial until a depth of about 20 m [5]. However, additional work is necessary

to evaluate effect of friction at depths greater than about 20 m. Alternatively, the hole could be cased for depths below 20 m to deal with this problem.

306

307

308

309

310

311

312

313

314

315

316

317

318

319

320

321

322

323

324

325

326

327

328

Plots of the energy-corrected N'_{120} values obtained from the light (63.5 kg) and heavy hammer (154 kg) have been provided for three different depth intervals (0-4 m, 4-8 m and beyond 8 m) in Fig. 17 to compare the agreement between the blow counts for the two different hammers at different depths. It should be noted that the data from Site 9 in Seward and some more points from other locations have been excluded from the data set as these data seem to be erroneous either due to inclined insertion of the penetration rod at the testing site or local variations in soil strata (as identified from uneven spikes in the N'_{120} plots). The best-fit regression line for all the data points ought to fall on the one-to-one line ideally to have perfect agreement indicating that the average DPT N'_{120} values are comparable after energy correction. The plots show that the correlation is reasonably good within 0 to 4m ($R^2 = 0.8$) and 4 to 8 m ($R^2 = 0.73$) depth with the trend line making a slope of 0.95. In addition, some scatter in these plots would be expected even if the same hammer energy was used at two adjacent soundings as a result of local variations in stratigraphy and gradation, especially in this variable glacial outwash environment. However, the correlation is relatively low ($R^2 = 0.69$) beyond 8 m depth with the regression line making a slope of 0.77 which clearly indicates that the light hammer is estimating relatively higher resistance compared to the heavy hammer.

To reduce the effects of uneven peaks and troughs on N'_{120} plots due to local variations in stratigraphy, particle size, and density, cumulative energy-corrected N'_{120} plots were produced for each pair of DPT soundings and are plotted versus depth for both light and heavy hammer DPT soundings in Figs. 5 through 16. These curves provide a better means of assessing the agreement in blow count between the two hammers. The slope of the cumulative curves also provide a

comparison of the variation as the slope at any point on the cumulative N'_{120} plot indicates the average in N'_{120} at that point. Therefore, the variation of slope along the cumulative N'_{120} plot indicates how the light and heavy hammer N'_{120} have been individually affected by different layers along the depth.

The light and heavy hammer cumulative blow counts match remarkably well at Site 5 in Valdez and Sites 10 and 12 at Seward despite showing considerable discrepancies in their respective N'_{120} plots. On the other hand, at Site 9 in Seward, the cumulative blow count of light hammer remains higher than the heavy hammer blow count starting from the ground surface because the vertical penetration could not be maintained for light hammer at this borehole.

At Sites 2 and 4 in Valdez and Site 11 in Seward, cumulative blow counts from the light and heavy hammers gradually deviate from each other beyond a depth of 8-10 m as was indicated by the plots in Fig. 17. Hence, the cumulative plots in Fig. 5 through 16 and the comparison between light and heavy hammer blow counts in Fig. 17 shows that uncertainty in the applicability of linear energy correction method gradually increases with depth especially for the light hammer penetrating the medium dense to dense gravelly deposits. To address this issue, a modification in the energy correction factor was determined for the light hammer by using the cumulative plots to provide the best agreement between the two cumulative N'_{120} curves at each individual site. Based on the gradual deviation, the percentage of error has been computed between the light and heavy hammer cumulative blow counts versus depth to obtain an average percentage of error for each site. Then the theoretical energy correction factor has been corrected by the average error percentage to obtain a modified energy correction factor for each site.

Fig. 18 shows the modified energy correction factors for all the locations in Valdez and Seward where both heavy and light hammers were used and also the deviation of the average

Eq. (1) and nominal values of drop height and weight). In all the cases except Site 9 and Site 11 in Seward, the correction factors are within about 10% of the theoretical correction factor suggesting relatively good agreement. As noted previously, the greater discrepancies are associated with sites where the DPT rods were not vertical during insertion. However, the DPT tests were all successfully conducted by the light hammer to the maximum depth of investigation, which in this study was 14 m. In addition, the fact that most of the adjusted energy correction points fall within 10% of the theoretical correction factor line in Fig. 18 suggest that the light hammer energy (that is used for SPT testing) can provide reasonable estimates of the N'_{120} blow count in profiles within relatively loose gravelly soils if care is taken to keep the drill rods close to vertical.

4. MASW TESTING AND INTERPRETATION

As part of this study, V_s profiles were developed using the Multichannel Analysis of Surface Waves (MASW) method near most DPT sites. The MASW method considers the dispersion of Rayleigh waves to generate an apparent phase-velocity vs. frequency relationship that is then used in an inversion analysis to derive a V_s profile. MASW surveys were performed using a linear array at each site composed of 16 vertical component 4.5 Hz geophones spaced at 1 m intervals to increase resolution near the surface and 3 m intervals to collect data at greater depths, as well as assist in interpreting higher modes in the measurements. At some site locations an additional array with 1 m interval was also conducted and was considered in the analysis. Efforts were made to ensure that the centerline of the arrays was the same and within meters from the location of the DPT. It should be noted that the V_s values were all obtained for free-field conditions as the investigated sites are not impacted by the topography or sloped ground conditions.

A 5.5 kg sledgehammer striking on a plastic plate was used as the seismic source. The source

was aligned to the geophones and was offset from the first geophone by 15-20% of the total array length. For each offset, a stack of five measurements was considered adequate to increase the signal-to-noise ratio.

375

376

377

378

379

380

381

382

383

384

385

386

387

388

389

390

391

392

393

394

395

396

The recorded phase offset of different frequency waves was used to develop a relationship between phase velocity and frequency (or wavelength), i.e., the dispersion curve. At each site, the low frequency dispersion curve was combined with high frequency curves to produce a composite dispersion curve. The two dispersion curves generally overlapped over the frequency of 15-20 Hz with one dispersion curve extending to higher frequencies (as high as 70 Hz) and the other to lower frequencies (as low as 5 Hz, but in some cases higher). At each site, initial inversion analyses were conducted using Park et al. [29] methodology, considering multiple modes when necessary and without a priori subsurface information to derive a shear wave velocity model. It is known that major differences in interpretation arise not from the dispersion analyses, but primarily from the inversion algorithm used to estimate the V_s profile from the dispersion curve. Therefore, the inversion process has a much stronger influence over the final V_s model compared to the dispersion curve generation method [30]. This increased variability in results during the inversion algorithm, arises because different V_s profiles may match the field data collected. To constrain the inversion process, additional inversion analyses were conducted using the stratigraphy observed from the DPT to generate a best-estimate V_s profile that was generally consistent (a) with the dispersion curve without necessarily forcing a "perfect" match, and (b) the DPT-based subsurface data.

Subsequently, the V_s values were corrected for overburden pressure to obtain $V_{s,1}$ using the equation:

$$V_{s,1} = V_s \left(P_a / \sigma'_{vo} \right)^{0.25} \tag{4}$$

where P_a is atmospheric pressure approximated by a value of 100 kPa as suggested by Sykora [31]

and adopted by Youd et al. [14].

The normalized $V_{s,I}$ profiles based on the MASW testing are plotted as a function of depth in Figs. 5 through 16. For Site 9 in Seward, cross-hole measurements were reported by Koester et al. [32] and are also shown in Fig. 13. Note that these measurements were not considered in the surface wave analyses, but the results are in relatively good agreement, with the highest variations in V_s being about 15% below 9 m depth where MASW-based V_s is around 15% lower than the cross-hole V_s . These variations are expected given the differences in experimental setups, wave propagation direction, the volume of soil material characterized using each technique (DPT in a borehole, 1 m spacing array and 3 m spacing array), as well as the uncertainties associated with data interpretation with both the MASW and cross-hole techniques.

5. COMPARISON WITH DPT BASED LIQUEFACTION TRIGGERING CURVES

The case histories in Alaska with DPT test results provide an excellent opportunity to evaluate the ability of the DPT-based liquefaction triggering curves developed by Cao et al. [5] to accurately predict liquefaction in gravelly soil. For both Valdez and Seward case histories, the geology, earthquake magnitude, and gravel layers are significantly different from those in the Chengdu plain of China and provide a good test of the method.

To evaluate the liquefaction potential with depth, the cyclic stress ratio (*CSR*) induced by the earthquake was computed using the simplified equation,

$$CSR = 0.65 (a_{max}/g) (\sigma_{vo}/\sigma'_{vo}) r_d$$
(5)

first proposed by Seed and Idriss [33] where a_{max} is the peak ground acceleration, σ_{vo} is the initial vertical total stress, σ'_{vo} is the initial vertical effective stress, and r_d is a depth reduction factor as defined by Youd et al. [14].

The original Cao et al. [5] triggering curves were developed for the single earthquake event

of M_w 7.9. Hence, to facilitate comparison with data points from earthquakes of different magnitude in the present study, the Cao et al. [5] data points and triggering curves were shifted upward to obtain the *CSR* values for a standard earthquake of M_w 7.5 (*CSR*_{M=7.5}) using the equation

$$CSR_{M=7.5} = CSR/MSF \tag{6}$$

where the Magnitude Scaling Factor (*MSF*) is given by the equation

$$MSF = 10^{2.24} / M_w^{2.56} \tag{7}$$

recommended by Youd et al. [14]. More recent magnitude scaling factor equations have been developed, but they typically require an assessment of relative density or include SPT or CPT penetration resistance which makes their applicability questionable or difficult to apply at gravel sites. The plots of $CSR_{M=7.5}$ for all the sites of Valdez and Seward are shown in Figs. 5 through 16 next to the plots of N'_{120} and $V_{s,1}$.

In this study, a_{max} values at Valdez and Seward were estimated to be 0.44g and 0.52g, respectively based on the peak ground acceleration values from the USGS Shakemap for the 1964 Great Alaskan earthquake [34]. Instrumental recordings for the earthquake are not available. USGS Shakemap incorporate a weighted-average approach for combining different types of data (e.g., recordings, intensities, ground motion prediction equations) to arrive at best estimates of peak ground motion parameters [34]. This methodology is consistent with the methodology followed by Boulanger and Idriss [35] who used Shakemap to make estimates of a_{max} for sites in their liquefaction case history database with no nearby recordings.

Based on the plots of N'_{120} and $CSR_{M=7.5}$, the critical layer for liquefaction was selected as the layer most likely to trigger and manifest liquefaction at the ground surface [5,7] at each site in this study. Typically, this is the gravel layer with the lowest average $N'_{120}/CSR_{M=7.5}$ below the water table which are associated with relatively high probabilities of liquefaction. It should be noted that

the critical layers have been selected based on the heavy hammer N'_{120} profiles as heavy hammer blow counts appear to be more consistent than the light hammer blow counts. Cohesive soil layers are excluded from consideration. If there are several layers found to be potentially liquefiable below the water table, priority is given to the layer which is the most probable to produce liquefaction manifestation on the surface. Hence, the depth and thickness of the selected critical layers are kept consistent with the observed liquefaction response [36] for all the liquefaction and no-liquefaction sites. Critical layers are typically selected over an interval of one meter or more to provide a more representative N'_{120} that is less affected by thin peaks or troughs [35]. Typically, the critical layers are also associated with the steeper slopes of the cumulative N'_{120} curves. Thus, the critical layers selected for each DPT profile based on all these considerations are indicated in Figs. 5 through 16. Additional soil and earthquake parameters for the critical liquefiable layers at these sites, e.g., total stress, effective stress, CSR and DPT blow counts are summarized in Table 1. It can be observed from the figures that majority of the critical layers remain in the range of 4-8 m or at shallower depth except site 8 at Valdez and site 10 at Seward where critical layer lies below 8 m depth.

440

441

442

443

444

445

446

447

448

449

450

451

452

453

454

455

456

457

458

459

460

461

462

The CSR and DPT N'_{120} for the critical layers at each site in Fig. 5 through 16 is plotted in Fig. 20 along with the triggering curves developed by Cao et al. [5] adjusted to M_w 7.5. In the plot, the solid red dots represent the sites where liquefaction occurred during the Wenchuan earthquake while the sites where no liquefaction took place are shown with open circles. Cao et al. [5] also defined curves indicating a 15, 30, 50, 70 and 85% probability of liquefaction based on logistical regression as shown in Fig. 20. As noted previously, the CSRs for these data points are some of the highest values in any existing liquefaction data set. The points from Old Valdez all plot above the 85% probability of liquefaction, while the points from Seward all fall on or above the 70%

probability of liquefaction, which is consistent with the actual case histories where liquefaction was observed at all sites. In contrast, the no-liquefaction sites in Valdez fall between the 30% and 50% triggering curves indicating a considerable chance of liquefaction which is inconsistent with the actual case history. Hence, the DPT based triggering curves developed by Cao et al. [5] evaluate the liquefaction potential of gravelly soils of Alaska with moderate accuracy. Further adjustment of these curves based on additional data points would be desirable to improve the method of evaluating liquefaction potential of gravelly soils.

6. COMPARISON WITH V_S -BASED LIQUEFACTION TRIGGERING CURVES

Liquefaction triggering curves based on shear wave velocity corrected for overburden stress $(V_{s,t})$ of sandy soils have been proposed by Andrus and Stokoe [16] and Kayen et al. [17] for sandy soils. According to Andrus and Stokoe [16], these curves, although developed for sandy soils, can be used on a preliminary basis for gravelly soils also, but they pointed out that "additional work is clearly needed to understand the relationship between $V_{s,t}$ and liquefaction resistance of gravels". In addition, Cao et al. [18] developed a set of probabilistic triggering curves for M_w 7.9 based on the gravel liquefaction case histories from the Chengdu plain in China during the Wenchuan earthquake in 2008. These triggering curves have been used in this study to evaluate the liquefaction potential of gravelly soils of Valdez and Seward. Sufficient data on gravel content was not available to evaluate liquefaction using the method given by Chang [5].

To perform the triggering analysis, first the critical layer for each site has been identified based on the plots of $V_{s,1}$ and $CSR_{M=7.5}$. Like the case of DPT, the critical $V_{s,1}$ layer is selected as that layer which has the lowest average range of $V_{s,1}/CSR_{M=7.5}$ indicating high probability of occurring liquefaction. The critical layer from the corrected shear wave velocity $(V_{s,1})$ profile at each site is shown in Fig. 5 through 16 and parameters are summarized in Table 1. As for the case

of DPT, the critical layers for $V_{s,I}$ have been selected over a thickness of one meter or more maintaining the consistency with the observed post-liquefaction response at the respective site [34].

Although the V_s -based critical layer is generally similar to that from the DPT in most cases, it is not identical. This is to be expected, as the thickness of the critical layer was not an input in constraining the inversion process of the surface wave analyses. Nevertheless, the critical layers are very similar in depth and thickness for seven out of nine sites where both shear wave velocity and DPT profiles are available, while they are different at two sites (Site 9 and Site 12 at Seward). There are several possible reasons for this apparent discrepancy, including the inherent variability of the site stratigraphy as indicated in the continuous DPT profiles and the differences between the two DPT profiles. In addition, the MASW technique samples a larger volume of material and yields an "average" estimate of V_s for the site, whereas the DPT provides an estimate of resistance in the immediate vicinity of the DPT. Hence, it is reasonable to have some degree of discrepancy between the interpreted soil profiles from two different methods. Although, the layering from the DPT was considered in the inversion process, it did not forcibly match the DPT and V_s -based critical layers.

The average fines content that has been used for obtaining the triggering curves shown in Fig. 21 for the methods of Andrus and Stokoe [16] and Kayen et al. [17] is 6% as per Alaska DOT site investigation reports. For each critical layer, the average $V_{s,l}$ was obtained while the average CSR for M_w 7.5 for every site was obtained using equations 4 and 5. Equation 6 was used to compute the MSF for both the methos of Andrus and Stokoe [16] and Cao et al. [18], as recommended by the 1997 NSF workshop participants [14]. For the method of Kayen et al. [17], specific equation for MSF was developed based on the respective database and the equation is

509 given by

$$MSF = 15M_w^{-1.34} \tag{10}$$

The CSRs and the corresponding $V_{s,I}$ values obtained from the critical layers for all the sites are plotted in Fig. 21 (a) and (b) relative to the triggering curves for sand proposed by Andrus and Stokoe[16] and Kayen et al. [17], respectively. Fig. 21a indicates that one liquefaction point from Valdez (Site 1) and two points from Seward (Sites 9 and 10) fall on the right-hand side of the triggering curve given by Andrus and Stokoe [16] indicating false prediction of no liquefaction. The remaining liquefaction and no-liquefaction points from both Valdez and Seward fall on the correct side of the triggering curve.

For the method of Kayen et al. [17] in Fig. 21b four points from Valdez (Sites 2, 3, 4 and 6) and two from Seward (Sites 11 and 12) where liquefaction took place, fall above the 85% triggering curve. However, two other points from Seward (Sites 9 and 10) and one from Valdez (Site 1) fall below the 15% triggering curve showing little chance of liquefaction despite the fact that significant liquefaction occurred at these sites. The results for the method of Cao et al. [18] are shown in Fig. 21(c) and all the points plot above the 85% probability of liquefaction which is consistent with the fact that liquefaction occurred at all these sites.

The results of this study indicate that the existing V_s -based triggering curves developed for sand by Andrus and Stokoe [16] and Kayen et al. [17] predicted no liquefaction at several gravelly soil sites in Valdez and Seward, Alaska, that did liquefy. This finding is consistent with V_s -based triggering analyses in gravelly soils in the 1976 M_w 7.6 Friuli earthquake [3] and the 2014 M_w 6.1 Cephalonia, Greece earthquake [6], and suggest that the triggering curves may need to shift to the right for gravelly soils. The triggering curves of Cao et al. [18] provide improved performance in evaluating the liquefaction potential; however, the data set for gravels is still relatively sparse.

Hence, it would be desirable to collect more V_s data points involving gravelly soils to improve the reliability of these triggering curves.

534

535

536

537

538

539

540

541

542

543

544

545

546

547

548

549

550

551

552

553

554

532

533

7. COMPARISON BETWEEN DPT AND V_S METHODOLOGIES

The DPT- and V_s -based liquefaction trigger approaches are completely different in-situ methods by nature. The former is a destructive test at large strain, while the latter is a nondestructive test as small strains. The DPT captures local variations in stratigraphy as the cone tip directly penetrates through the gravelly deposits to measure the soil resistance. On the other hand, V_s methodologies provide an average shear wave velocity for a certain depth interval by either measuring the arrival time of a shear wave, or in the case of MASW interpreting Rayleigh wave propagation, that may not capture all the local variations in a soil stratum. Therefore, both resolution and representative volume for each measurement are different, and one may not be considered necessarily more correct than other, especially in gravelly soils. Therefore, the plots in Figs. 5 through 16 shows that the profiles of the DPT blow counts (N'_{120}) contain more detailed variations in penetration resistance with several peaks and troughs along the depth whereas the V_{sI} profiles are smoother reflecting average responses of various soil strata. However, the overall pattern of N'_{120} and $V_{s,1}$ profiles are generally consistent with each other for most of the sites except sites 9 and 10 in Seward where a few local variations might not have been captured by the MASW. Overall, the consistency between the N'_{120} and $V_{s,1}$ profile indicates the reliability of each method in characterizing the gravelly deposits. In addition, the probability of liquefaction plots based on the N'_{120} and $V_{s,1}$ methods are also quite consistent for most sites except for some local variations. Accordingly, the depth and thickness of the critical layers are not always identical (nor should they be expected to be) but are consistent for most sites except sites 9 and 12 at Seward due to the

inherent variations in the local stratigraphy.

8. CONCLUSIONS

Based on the investigations conducted using the Dynamic Cone Penetrometer Test (DPT) and shear wave velocity logging in gravelly soils at Valdez and Seward, Alaska, the following conclusions are drawn:

- 1. The DPT-based liquefaction triggering curves developed by Cao et al. (2013) correctly evaluated the liquefaction potential for all the sites in Old Valdez and Seward. The points from Old Valdez all lie above the 85% probability curve and the points from Seward are all located on or above the 70% probability curve. These evaluations are consistent with liquefaction occurrence in gravel deposits at these sites during the 1964 Alaska earthquake. However, at two sites in Valdez where liquefaction did not occur during the earthquake, the *CSR-N'120* points lie between the 30% and 50% probabilistic triggering curves. Although the data points are below the 50% boundary, the probability of liquefaction is still higher than might be expected. These results suggest the need for additional data and regression analyses to improve the Cao et al. (2013) triggering curves that were developed for the Wenchuan earthquake.
- 2. The $V_{s,I}$ -based liquefaction triggering curves for sands proposed by Andrus and Stokoe (2000) and Kayen et al. (2013) predicted no liquefaction at sites in Alaska where gravels did actually liquefy. These results suggest that triggering curves for gravels should be adjusted to the right relative to triggering curves for sands as suggested by Rollins et al. (2020), Athanasopoulos-Zekkos et al. (2019) and Chang (2016). The $V_{s,I}$ -based triggering curves developed by Cao et al. (2011) based on gravel liquefaction case histories correctly evaluated the liquefaction potential for all the sites in Alaska.
 - 3. Typical hammer energy correction factors provide a reasonable means for adjusting the

heavy or light hammer blow counts to the conventional Chinese hammer blow counts. Modifications in hammer energy correction factors of $\pm 10\%$ typically produced relatively consistent cumulative blow count curves from the light and heavy hammers in the loose gravelly profiles investigated during this study when the DPT rod was kept relatively vertical.

DATA AVAILABILITY

Some or all data, models, or code that support the findings of this study are available by the authors upon reasonable request. These data include electronic versions of the V_s and DPT logs, cumulative DPT logs, and probability of liquefaction curves. Supplemental data regarding the MASW dispersion curves are included with this paper.

ACKNOWLEDGEMENTS

Financial support for this study was provided by grants CMMI-1663546 and CMMI-1663288 from the National Science Foundation and grant G16AP00108 from the US Geological Survey Earthquake Hazard Reduction Program. This funding is gratefully acknowledged. However, the opinions, conclusions and recommendations in this paper do not necessarily represent those of the sponsors. We also express appreciation to Tim Weiss and David Hemstreet of the Alaska Department of Transportation for providing drilling services at significantly reduced cost and to We also wish to thank the cities of Seward and Valdez for allowing access to perform the DPT testing.

601 **REFERENCES**

- 602
- 603 [1] Coulter, H.W., and Migliaccio, R.R. 1966. "Effect of the Earthquake of March 22, 1964 at
- Valdez. Alaska." U.S. Geological Survey Professional Paper 542-C.
- 605 [2] McCulloch, D. S., & Bonilla, M. G. 1970. "Effects of the earthquake of March 27, 1964, on
- the Alaska Railroad". US Government Printing Office.
- 607 [3] Rollins, K.M., Amoroso, S., Milan, G., Minerelli, L., Vassallo, M., Di Giulio, G. 2020.
- "Gravel liquefaction assessment using the dynamic cone penetration test based on field
- performance from the 1976 Friuli earthquake." J. Geotechnical & Geoenvironmental
- Engrg., ASCE, https://DOI.org/10.1061/(ASCE)GT.1943-5606.0002252.
- 611 [4] Andrus, R.D. 1994. "In situ characterization of gravelly soils that liquefied in the 1983 Borah
- Peak earthquake." *Ph.D. Dissertation*, Civil Engineering Dept., Univ. of Texas at Austin,
- 613 579 pp.
- [5] Cao, Z., Youd, T., and Yuan, X. 2013. "Chinese Dynamic Penetration Test for liquefaction
- evaluation in gravelly soils." *J. Geotech. Eng.*, 10.1061/(ASCE)GT.1943-5606.0000857.
- 616 [6] Athanasopoulos, G. A., Kechagias, G. C., Zekkos, D., Batilas, A., Karatzia, X., Lyrantzaki,
- F., & Platis, A. 2020. Lateral spreading of ports in the 2014 Cephalonia, Greece,
- earthquakes. Soil Dynamics and Earthquake Engineering, 128, 105874.
- [7] Dhakal, Riwaj, Misko Cubrinovski, Jonathan Bray, and Christopher de la Torre. 2020.
- "Liquefaction assessment of reclaimed land at Centreport, Wellington." Bulletin of the New
- *Zealand Society for Earthquake Engineering* 53, no. 1: 1-12.
- 622 [8] Harder, L.F. 1997. "Application of the Becker Penetration Test for evaluating the
- 623 liquefaction potential of gravelly soils." NCEER Workshop on Evaluation of Liquefaction
- *Resistance*, held in Salt Lake City, Utah.

- 625 [9] DeJong, J.T., Ghafghazi, M., Sturm, A.P., Wilson, D.W., den Dulk, J., Armstrong, R.J.,
- Perez, A., and Davis, C.A. 2017. "Instrumented Becker Penetration Test. I: Equipment,
- Operation, and Performance." J. Geotech. Eng., doi.org/10.1061/(ASCE)GT.1943-
- 628 5606.0001718.
- [10] Harder, L.F. 1988. "Use of penetration tests to determine the cyclic loading resistance of
- gravelly soils during earthquake shaking." Ph.D. Dissertation, Civil Engineering Dept.,
- Univ. of California, Berkeley, CA., Vol. 2, 242 p.
- [11] Meyerhof, G.G. 1957. "Discussion on Research on determining the density of sands by
- spoon penetration testing". In Proceedings, 4th International Conference on Soil Mechanics
- *and Foundation Engineering*. London, Vol.3, p. 110.
- [12] Iqbal, M. S., Robertson, P. K., and Sego, D. C. 2004 "Discrete element modeling of cone
- penetration testing in coarse grain soils." (2000): 0917-0917.
- 637 [13] Chinese Design Code 2001. "Design Code for building foundation of Chengdu region."
- Administration of Quality and Technology supervision of Sichuan Province PRC (in
- 639 Chinese), DB51/T5026-2001.
- [14] Youd, T.L., Idriss, I.M., Andrus, R.D., Arango, I., Castro, G., Christian, J.T., Dory, R., Finn,
- W.D.L., Harder, L.F., Hynes, M.E., Ishihara, K., Koester, J.P., Liao, S.S.C., Marcuson,
- W.F., Martin, G.R., Mitchell, J.K., Moriwaki, Y., Power, M.S., Robertson, P.K., Seed, R.B.,
- and Stokoe, K.H. 2001. "Liquefaction resistance of soils: Summary Report from the 1996
- NCEER and 1998 NCEER/NSF Workshops on evaluation of liquefaction resistance of
- soils." J. Geotech. Eng., 10.1061/(ASCE)1090-0241(2001)127:10(817).
- 646 [15] Cubrinovski, Misko, Jonathan D. Bray, Christopher de la Torre, Michael Olsen, Brendon
- Bradley, Gabriele Chiaro, Emilia Stocks, Liam Wotherspoon, and Tiffany Krall. 2018.

- "Liquefaction-Induced Damage and CPT Characterization of the Reclamations at
- CentrePort, Wellington Liquefaction-Induced Damage and CPT Characterization of the
- Reclamations at CentrePort, Wellington." Bulletin of the Seismological Society of
- 651 *America,* 108(3B): 1695-1708.
- 652 [16] Andrus, R.D., and Stokoe, K.H., II 2000. "Liquefaction resistance of soils from shear-wave
- velocity." J. Geotech. Eng., 10.1061/(ASCE)1090-0241(2000)126:11(1015).
- [17] Kayen, Robert, R. E. S. Moss, E. M. Thompson, R. B. Seed, K. O. Cetin, A. Der Kiureghian,
- Y. Tanaka, and K. Tokimatsu. (2013) "Shear-wave velocity-based probabilistic and
- deterministic assessment of seismic soil liquefaction potential." *Journal of Geotechnical and*
- *Geoenvironmental Engineering* 139, no. 3: 407-419.
- 658 [18] Cao, Z., Youd, T.L., and Yuan, X. 2011. "Gravelly soils that liquefied during 2008
- Wenchuan, China Earthquake, Ms = 8.0." Soil Dynamics and Earthquake Engineering,
- 660 31(8), 1132-1143.
- [19] Chang, W.J. 2016. "Evaluation of liquefaction resistance for gravelly sands using gravel
- content-corrected shear-wave velocity." J. Geotech. Eng., 10.1061/(ASCE)GT.1943-
- 663 5606.0001427.
- [20] Moffit, F. H. 1954. "Geology of the Prince William Sound Region, Alaska." U.S. Geological
- 665 Survey Bulletin, 989-E, 225-310.
- 666 [21] Winkler, G. R., Miller, R. J., MacKevett Jr, E. M., & Holloway, C. D. 1980. "Map and
- summary table describing mineral deposits in the Valdez quadrangle, southern Alaska." *U.S.*
- 668 Geological Survey Open-File Report (No. 80-892-B).
- 669 [22] Shannon and Wilson, Inc. Report on subsurface investigation for Mineral Creek townsite,
- city of Valdez, Alaska, to U.S. Army Engineer District, Anchorage, Alaska, Seattle:

- Shannon and Wilson, Inc., pp. 34-77, 1964.
- 672 [23] Lee, H.J., Lee, Ryan, H., Haeussler, P.J., Kaye, R.E., Hampton, M.A., Locat, J. 2007.
- 673 "Reassessment of seismically induced, tsunamigenic submarine slope failures in Port
- Valdez, Alaska, USA." Submarine Mass Movements and Their Consequences, Springer,
- 675 357-365.
- 676 [24] Parsons, Tom, Eric L. Geist, Holly F. Ryan, Homa J. Lee, Peter J. Haeussler, Patrick Lynett,
- Patrick E. Hart, Ray Sliter, and Emily Roland. "Source and progression of a submarine
- landslide and tsunami: The 1964 Great Alaska earthquake at Valdez." Journal of
- 679 *Geophysical Research: Solid Earth* 119, no. 11 (2014): 8502-8516.
- [25] Youd, T.L. 2014. "Ground failure investigations following the 1961 Alaska Earthquake."
- Proc. 10th US National Conf. on Earthquake Engrg., Earthquake Engineering Research
- Institute, DOI: 10.4231/D3DN3ZW6P.
- [26] She, K., Horn, D. P. D. P., and Canning, P., 2006, "Porosity and hydraulic conductivity of
- 684 mixed sand-gravel sediment." Proc., 41st Defra Conf. on Flood and Coastal Risk
- Management, p. 1-16. HR Wallingford, Oxford, UK
- 686 [27] Cao, Z., Yuan, X., Youd, T.L., and Rollins, K.M. 2012. "Chinese Dynamic Penetration tests
- (DPT) at liquefaction sites following 2008 Wenchuan Earthquake." *Proc.*, 4th Int. Conf. on
- Geotechnical and Geophysical Site Characterization, Taylor & Francis Group, London,
- 689 1499-1504.
- 690 [28] Seed, H., Kohji Tokimatsu, L. F. Harder, and Riley M. Chung. "Influence of SPT procedures
- in soil liquefaction resistance evaluations." *Journal of geotechnical engineering* 111, no. 12
- 692 (1985): 1425-1445.
- 693 [29] Park, C.B., Miller, R.D, and Xia J. 1999. "Multichannel analysis of surface waves."

- 694 Geophysics, 64: 800–808. Parsons, T., Geist, E.L., Ryan, H.F., Lee, H.F., Haeussler, P.J.,
- Lynett, P., Hart, P.E., Sliter, R., and Roland, E. (2014). "Source and progression of a
- submarine landslide and tsunami: The 1964 Great Alaska earthquake at Valdez." J.
- 697 Geophysical Research: Solid Earth, AGU publications, American Geophysical Union,
- 698 8502-8516, DOI: 10.1002/2014JB011514.
- 699 [30] Garofalo, F., Foti, S., Hollender, F., Bard, P. Y., Cornou, C., Cox, B. R., Ohrnberger, M.,
- Sicilia, D., Asten, M., Di Giulio, G., Forbriger, T., Guillier, B., Hayashi, K., Martin, A.,
- Matsushima, S., Mercerat, D., Poggi, V., and Yamanaka, H. 2016. "InterPACIFIC Project:
- Comparison of Non-Invasive Methods for Seismic Site Characterization. Part I: Intra-
- Comparison of Surface Wave Methods." Soil Dynamics and Earthquake Engineering, 82,
- 704 222-240.
- 705 [31] Sykora, D. W. 1987. "Creation of a data base of seismic shear wave velocities for correlation
- analysis." Geotech. Lab. Misc. Paper GL-87-26, U.S. Army Engr. Waterways Experiment
- 707 Station, Vicksburg, Miss.
- Koester, J.P., Daniel, C. and Anderson, M. 2000. "In situ investigation of liquefied gravels:
- at Seward Alaska." Innovations and Applications in Geotechnical Site Characterization,
- Geotechnical Special Publication 97, ASCE, p. 33-48.
- 711 [33] Seed, H.B. and Idriss, I.M. 1971. "Simplified procedure for evaluating soil liquefaction
- 712 potential." J. Soil Mechanics and Foundations Div., ASCE, 97(SM9), 1249-1273.
- 713 [34] Worden, C.B., E.M. Thompson, M. Hearne, and D.J. Wald. (2020). ShakeMap V4 Manual:
- technical guide, user's guide, and software guide, U. S. Geological Survey.
- 715 http://usgs.github.io/shakemap/index.html sampled Feb 28, 2020.
- 716 [35] Boulanger, R.W. and Idriss, I.M. 2014. "CPT and SPT based liquefaction triggering

717		procedures." Report No. UCD/CGM-14/01, Center for Geotechnical Modeling, Dept. of
718		Civil and Environ. Engrg. Univ. of CalifDavis, 134 p.
719	[36]	Green, R. A., and S. M. Olson. 2015. "Interpretation of liquefaction field case histories for
720		use in developing liquefaction triggering curves." In Proc. 6th Intern. Conf. on Earthquake
721		Geotechnical Engineering.
722		
723		
724		
725		
726		
727		

Table 1. Summary of average soil and earthquake properties at Valdez and Seward

Site		Latitude	Longitude	GWT (m)	Critical Layer Depth (m)	Critical Layer Thickness (m)	Avg. Gravel Content (%)	Avg. Sand Content (%)	Avg.	Avg. σ_{vo} (kPa)	Avg. σ'_{vo} (kPa)	Avg. N' ₁₂₀	Avg. $V_{s,I}$ (m/s)	PGA (g)	Avg. CSR	Liquefaction occurred?
	1	61°6'28.73" N	146°14'16.12" W	0.7	8.8 (10)	1.2 (1)	34	66	27.7	183.7 (211.3)	104.4 (119.2)	12.3	242	0.44	0.47 (0.46)	Yes
	2	61°6'51.33" N	146°16'5.98" W	1	6.5	1.5	34	66	27.7	141.3	84.5	9.2	144	0.44	0.45	Yes
Old	3	61°6'53.67" N	146°16'11.06" W	0.8	3.5	1	34	66	27.7	94.7	57.5	7.8	185	0.44	0.45	Yes
Valdez	4	61°6'55.87" N	146°16'0.77" W	1	2.5 (5.5)	1.2	34	66	27.7	52.3 (115.9)	36.6 (70.8)	16.1	189	0.44	0.39 (0.44)	Yes
	5	61°6'51.12" N	146°16'19.20" W	0.7	2.7	1.5	34	66	27.7	71.3	43.9	5.1	-	0.44	0.45	Yes
	6	61°6'53.28" N	146°15'57.96" W	1	7	1.5	34	66	27.7	147.7	87.9	9.1	136	0.44	0.45	Yes
	7	61°7'43.10" N	146°21'36.10" W	3.4	8.6		45	55	22.9	182.4	130.6	20.7	-	0.44	0.37	No
Valdez	8	61°7'51.8" N	146°21'36.20" W	3.4	7.5		45	55	22.9	154.4	115.5	21.4	-	0.44	0.36	No
	9	60°8'29.27" N	149°25'8.24" W	3	7.5 (10)	1.3 (1.3)	64	36	47.1	156.7 (212.7)	111.9 (142)	13.8	215	0.52	0.43 (0.44)	Yes
C 1	10	60°8'33.99" N	149°25'16.16" W	4.9	7 (10.5)	1.2 (1.2)	64	36	47.1	155.3 (219.9)	128.4 (163.1)	18.6	251	0.52	0.37 (0.39)	Yes
Seward	11	60°8'12.27" N	149°25'19.8" W	1.6	2.4		64	36	47.1	52.6	42.7	7.6	200	0.52	0.39	Yes
	12	60°8'26" N	149°25'11.61" W	1.6	2.5		64	36	47.1	63.5	48.6	5.4	170	0.52	0.41	Yes

731 N.B. - The values in parentheses are those for critical V_{sI} layers where they are significantly different than those for critical DPT N'_{120} layers.

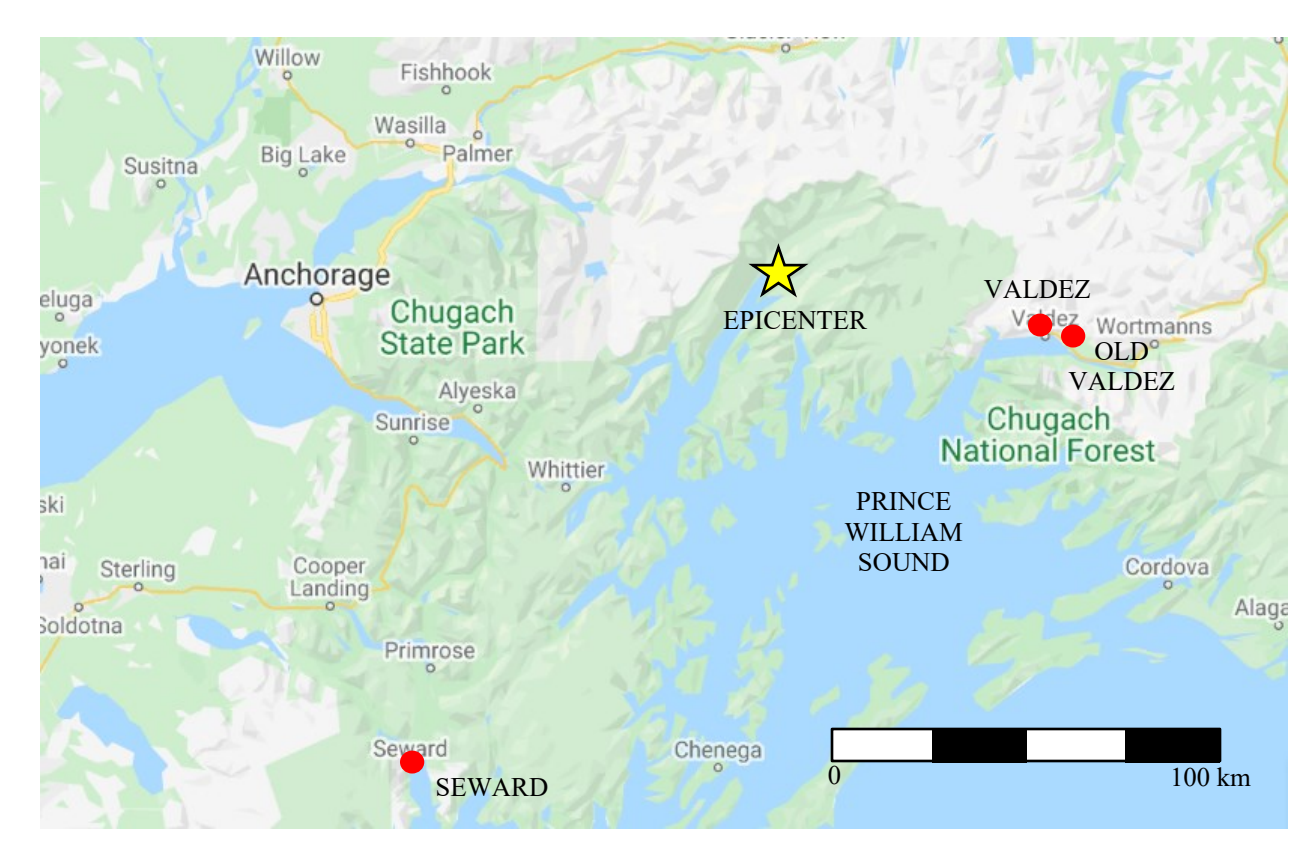


Fig. 1. Site map showing locations of Seward, Old Valdez and Valdez relative to the Epicenter of the $1964~M_w9.2$ Alaska Earthquake.

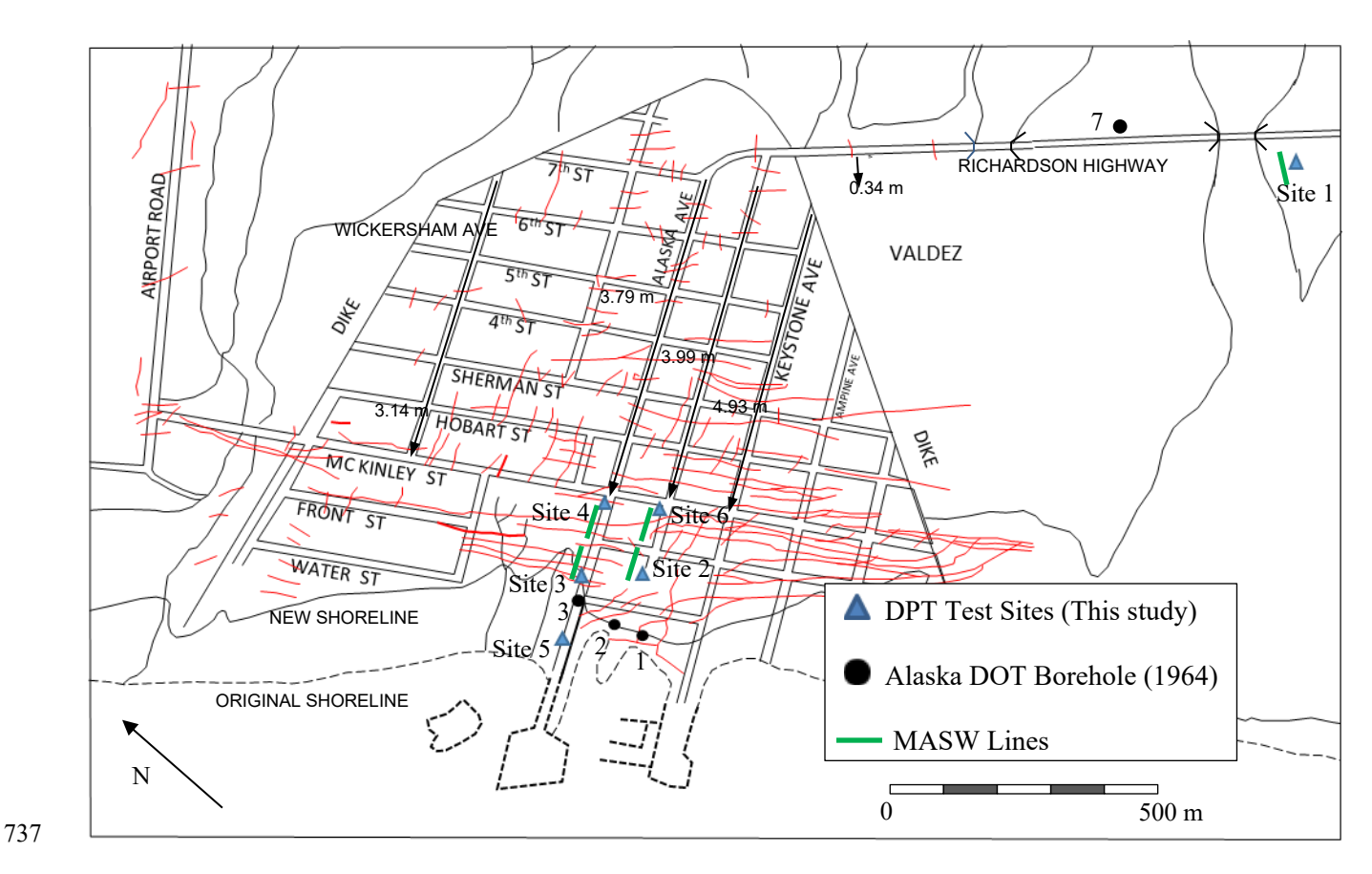
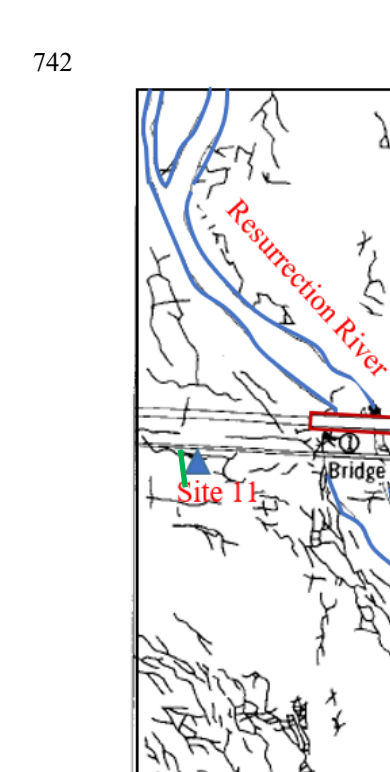


Fig. 2. Locations of boreholes made by USGS and Alaska DOT near the seacoast (modified from Coulter and Migliaccio, 1966) at Old Valdez. Dashed lines show original shoreline and piers prior to landslide and red curves show fissures from lateral spread towards the free face.



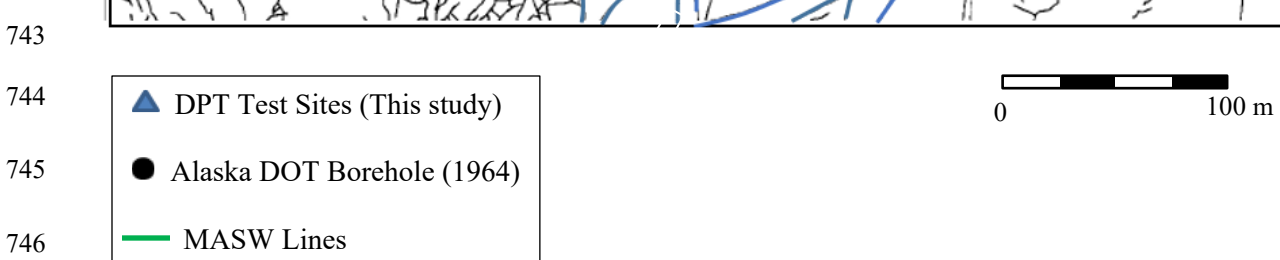


Fig. 3. Location of DPT investigation sites and penetration boreholes by Alaska DOT at Seward (based on McCulloch and Bonilla, 1964)

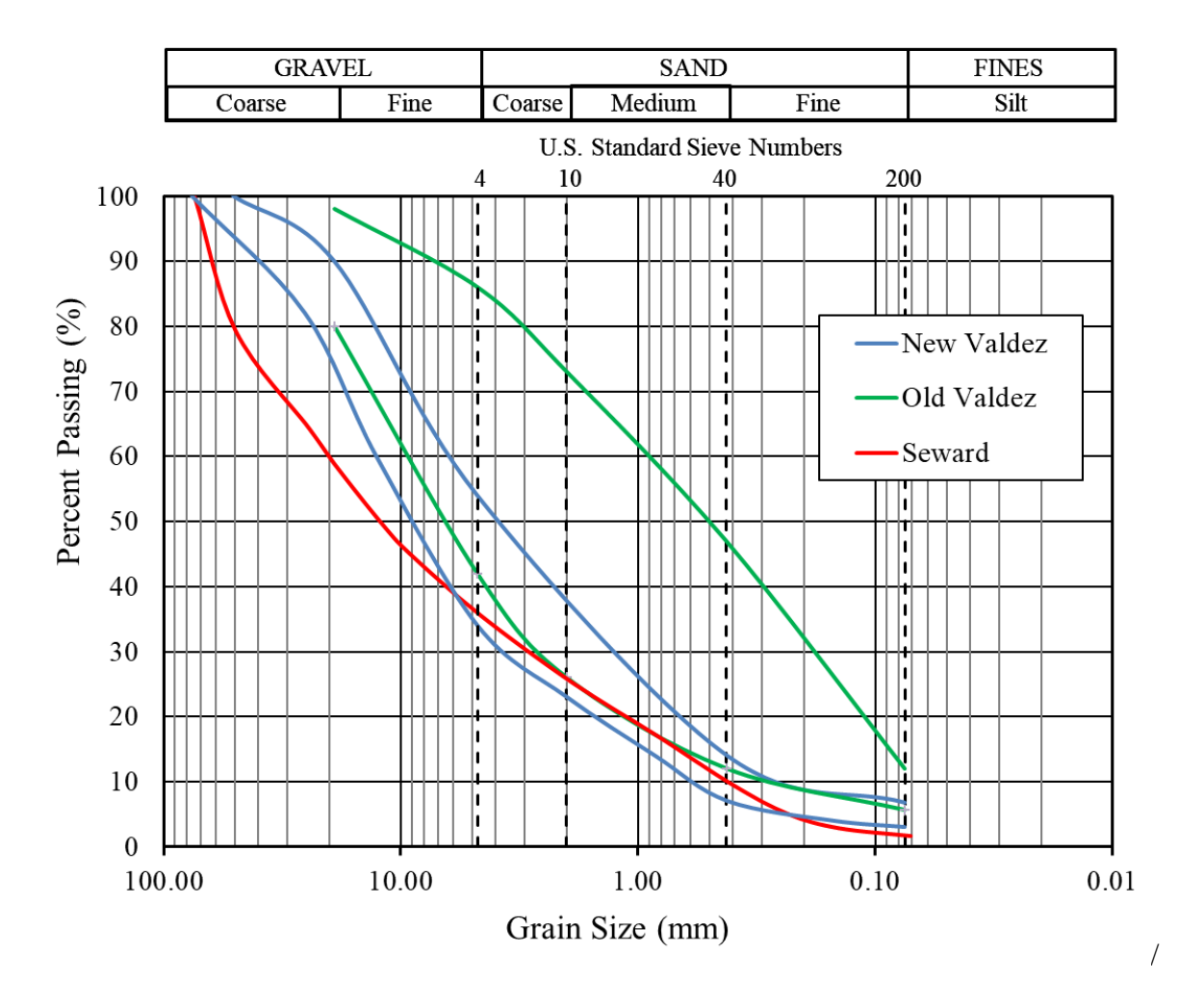


Fig. 4. Average grain size distribution curves for Old Valdez, Valdez and Seward

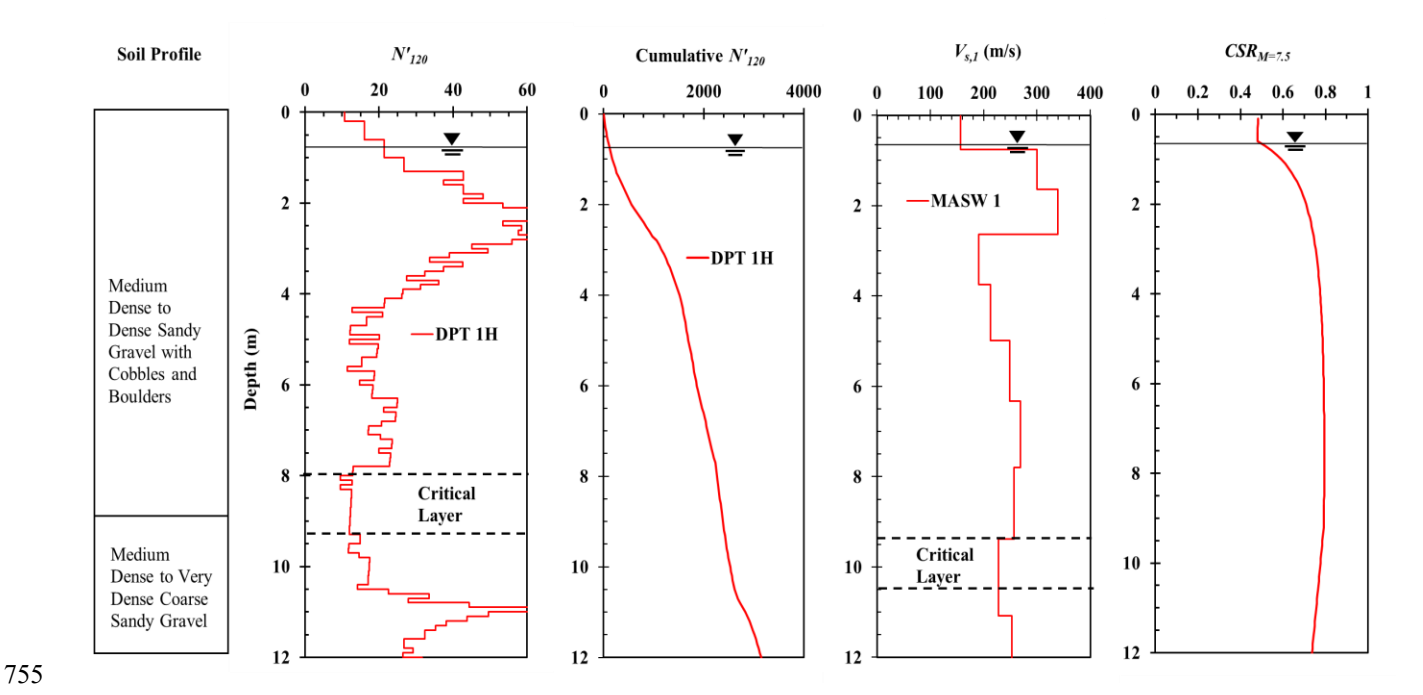


Fig. 5. Profile of soil strata, DPT N'_{120} and cummulative DPT N'_{120} for 154 kg hammer (H), $V_{s,1}$ and $CSR_{M=7.5}$ for Site 1 at Old Valdez.

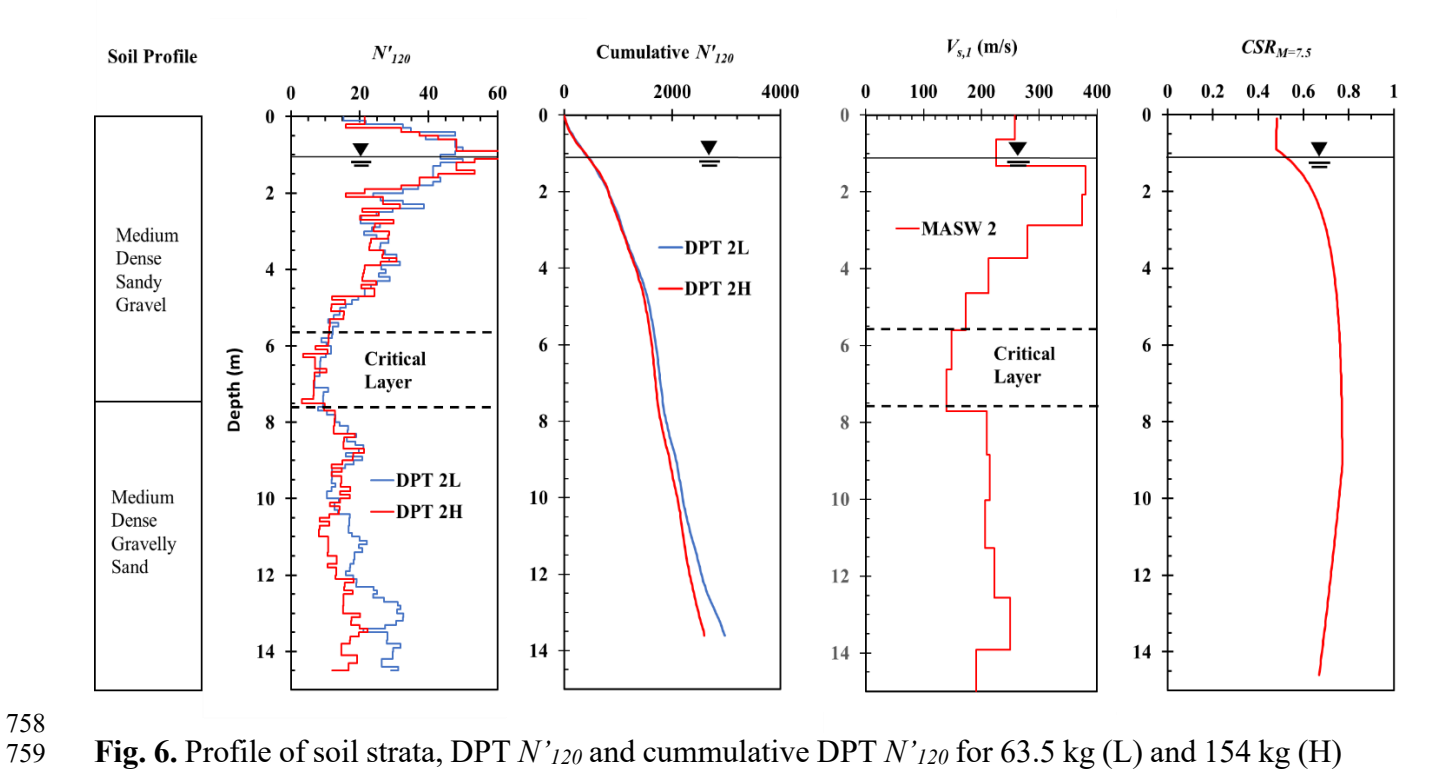


Fig. 6. Profile of soil strata, DPT N'_{120} and cumulative DPT N'_{120} for 63.5 kg (L) and 154 kg (H) hammer, $V_{s,1}$ and $CSR_{M=7.5}$ for Site 2 at Old Valdez.

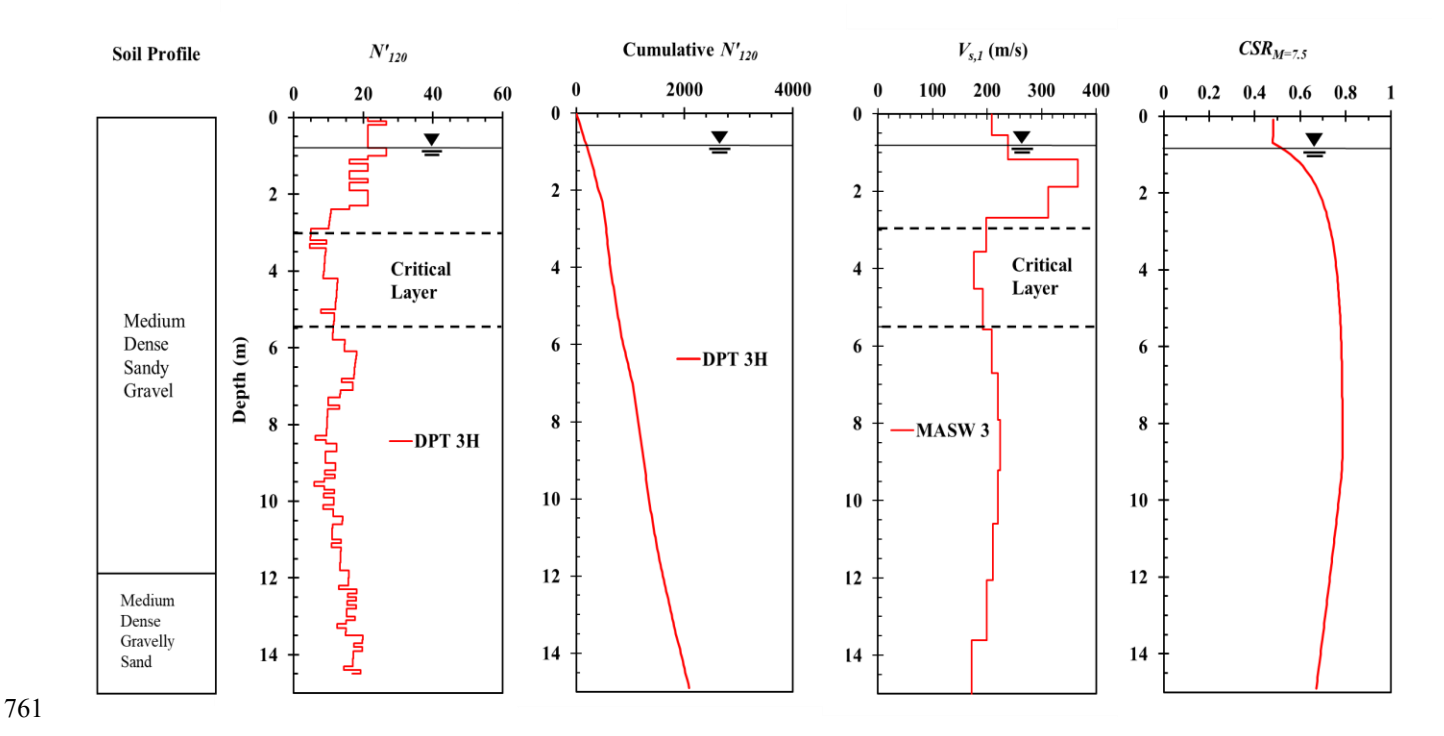


Fig. 7. Profile of soil strata, DPT N'_{120} and cummulative DPT N'_{120} for 154 kg hammer (H), $V_{s,1}$ and $CSR_{M=7.5}$ for Site 3 at Old Valdez.

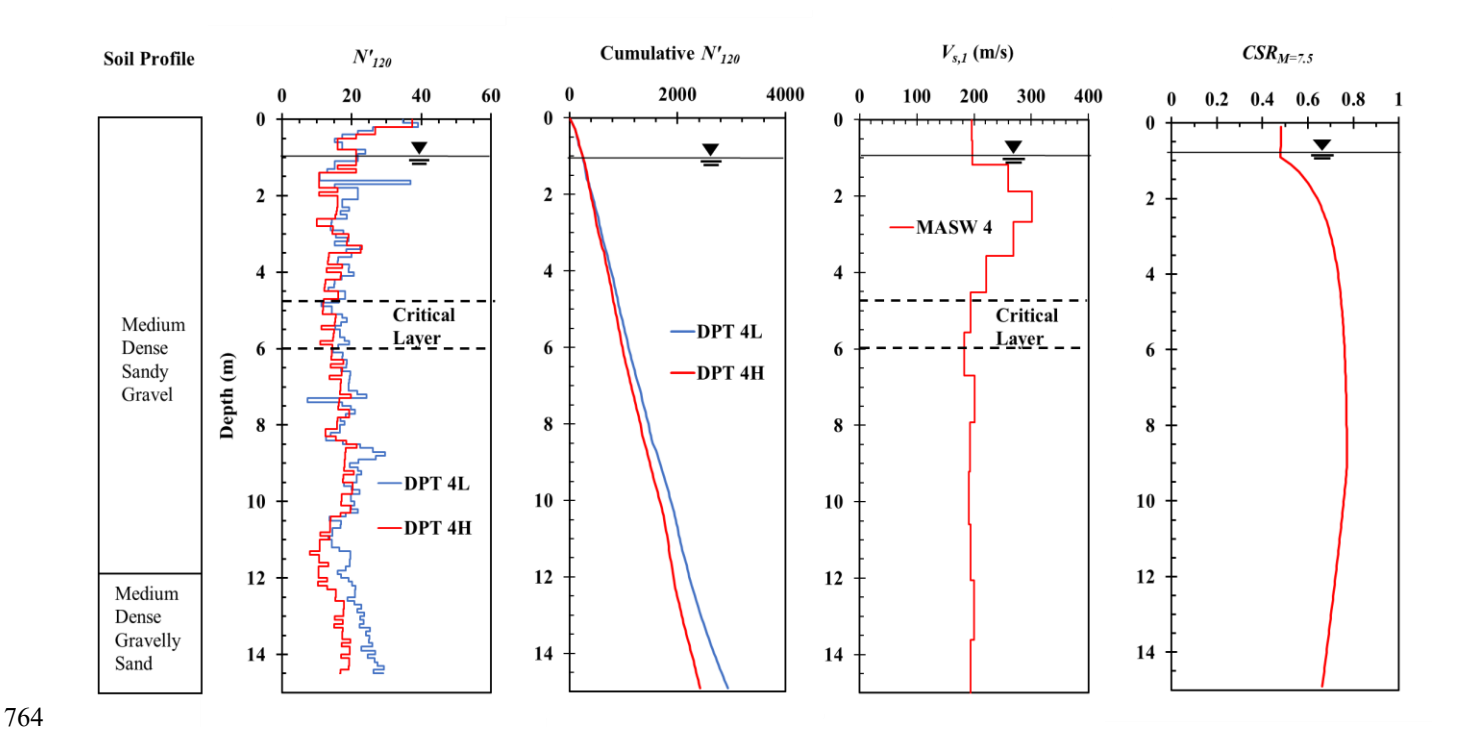


Fig. 8. Profile of soil strata, DPT N'_{120} and cummulative DPT N'_{120} for 63.5 kg (L) and 154 kg (H) hammer, $V_{s,1}$ and $CSR_{M=7.5}$ for Site 4 at Old Valdez.

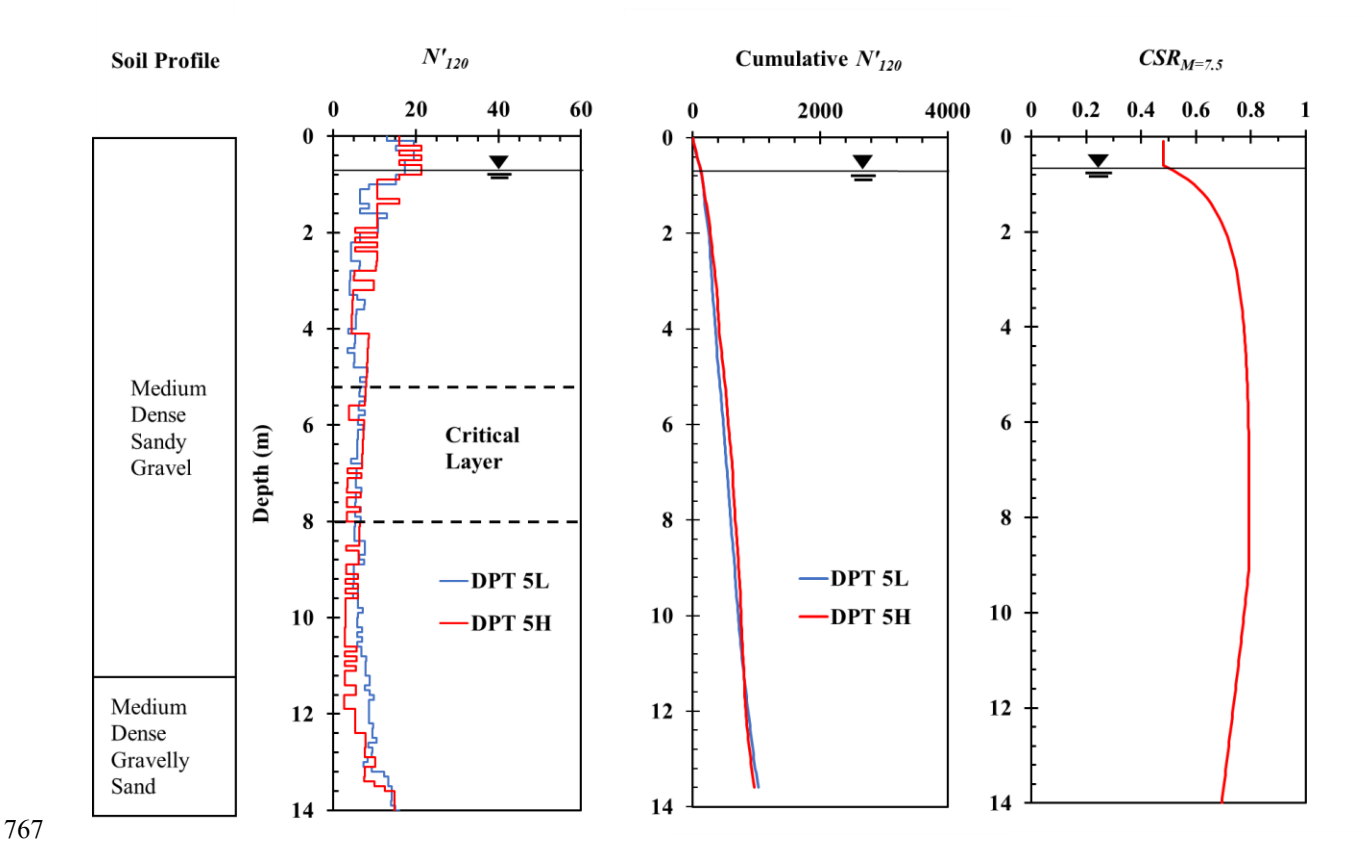


Fig. 9. Profile of soil strata, DPT N'_{120} and cummulative DPT N'_{120} for 63.5 kg (L) and 154 kg (H) hammer, and $CSR_{M=7.5}$ for Site 5 at Old Valdez.

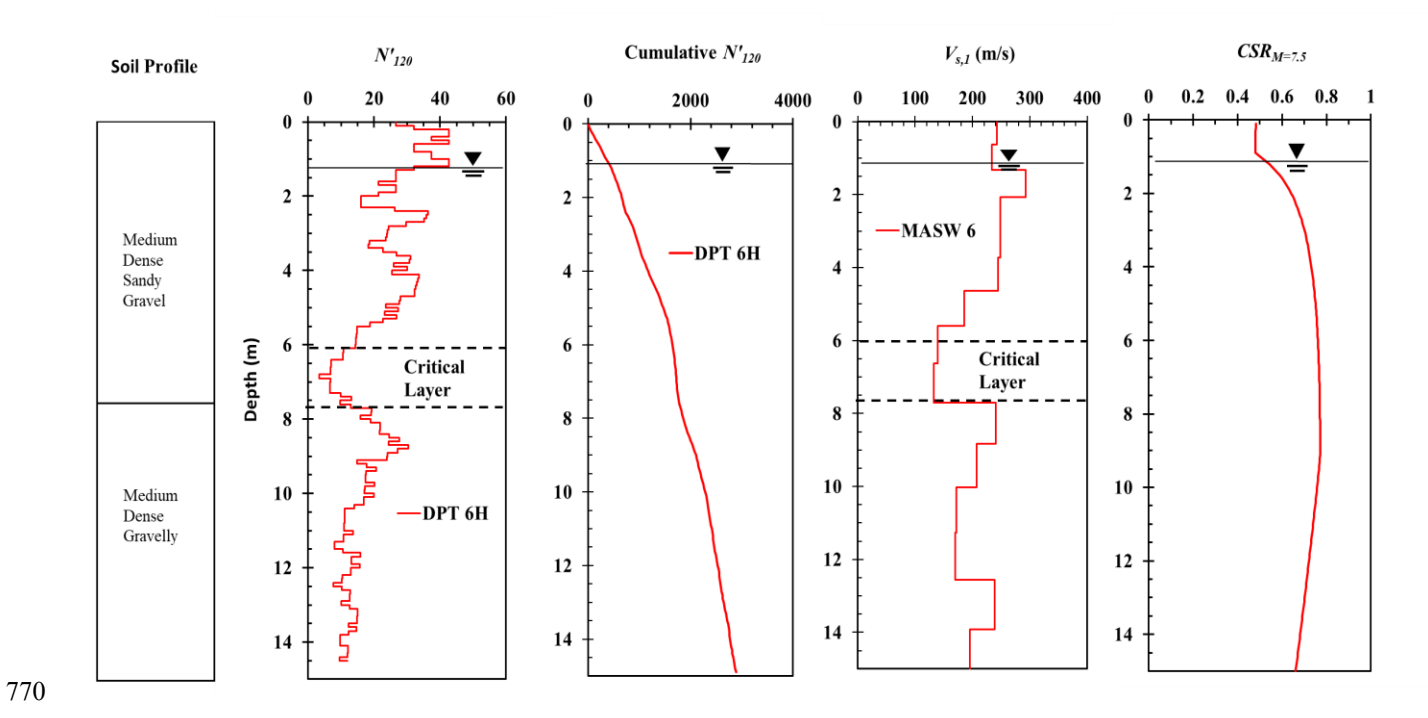


Fig. 10. Profile of soil strata, DPT N'_{120} and cummulative DPT N'_{120} for 154 kg hammer (H), $V_{s,1}$ and $CSR_{M=7.5}$ for Site 6 at Old Valdez.

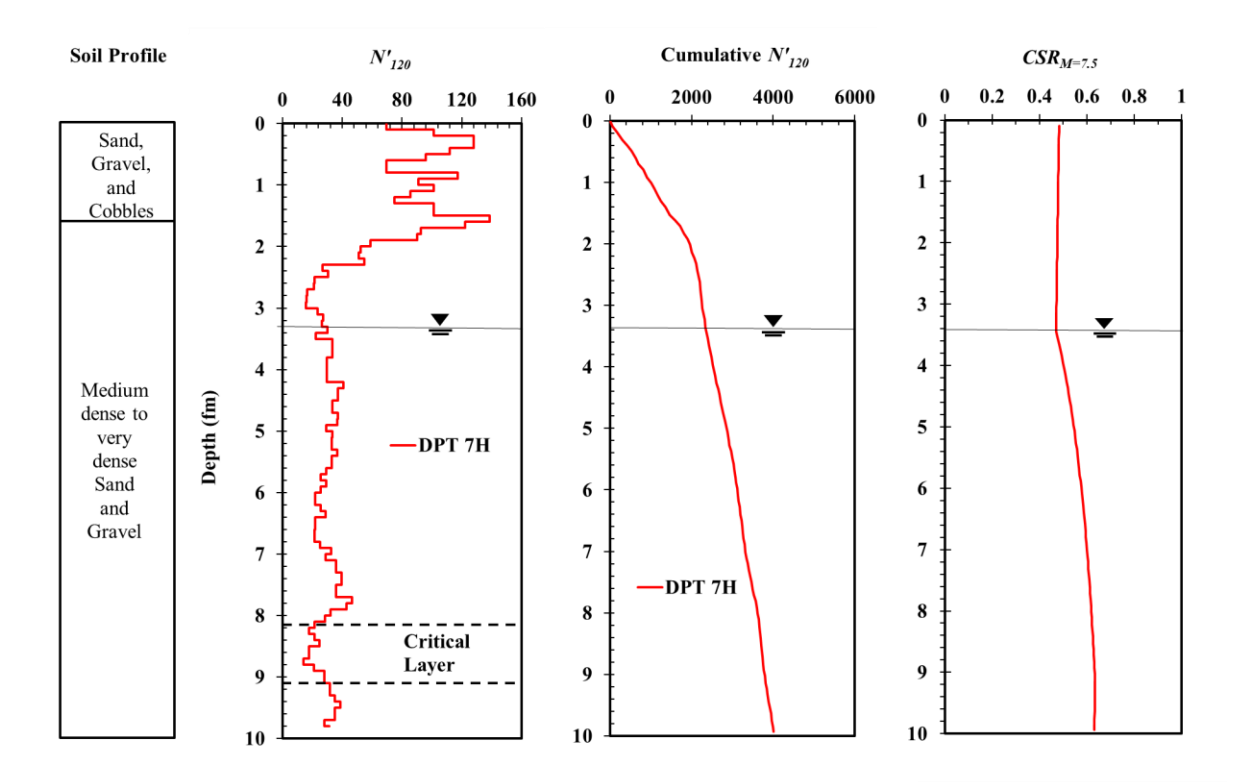


Fig. 11. Profile of soil strata, DPT N'_{120} and cummulative DPT N'_{120} for 63.5 kg (L) and $CSR_{M=7.5}$ for Site 7 at Valdez.

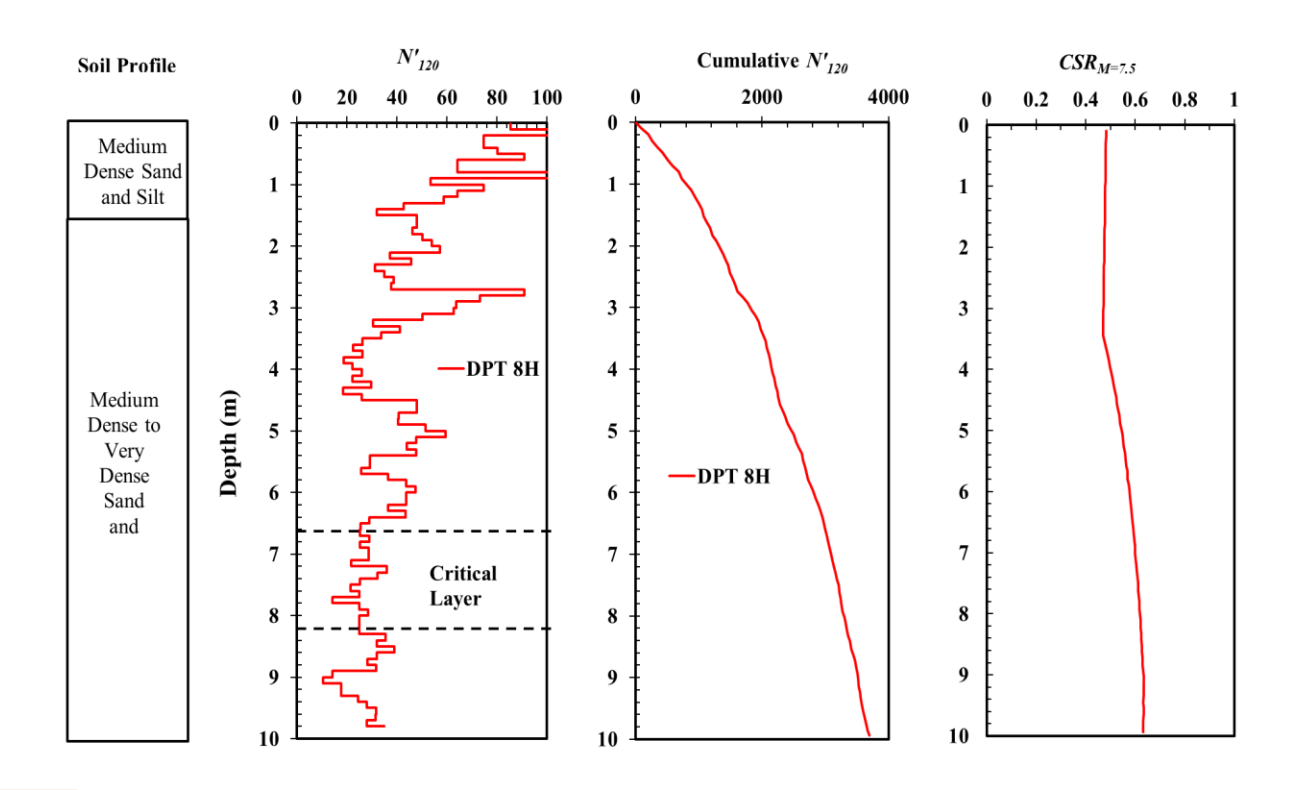


Fig. 12. Profile of soil strata, DPT N'_{120} and cumulative DPT N'_{120} for 63.5 kg (L) and $CSR_{M=7.5}$ for Site 8 at Valdez.

779 mi

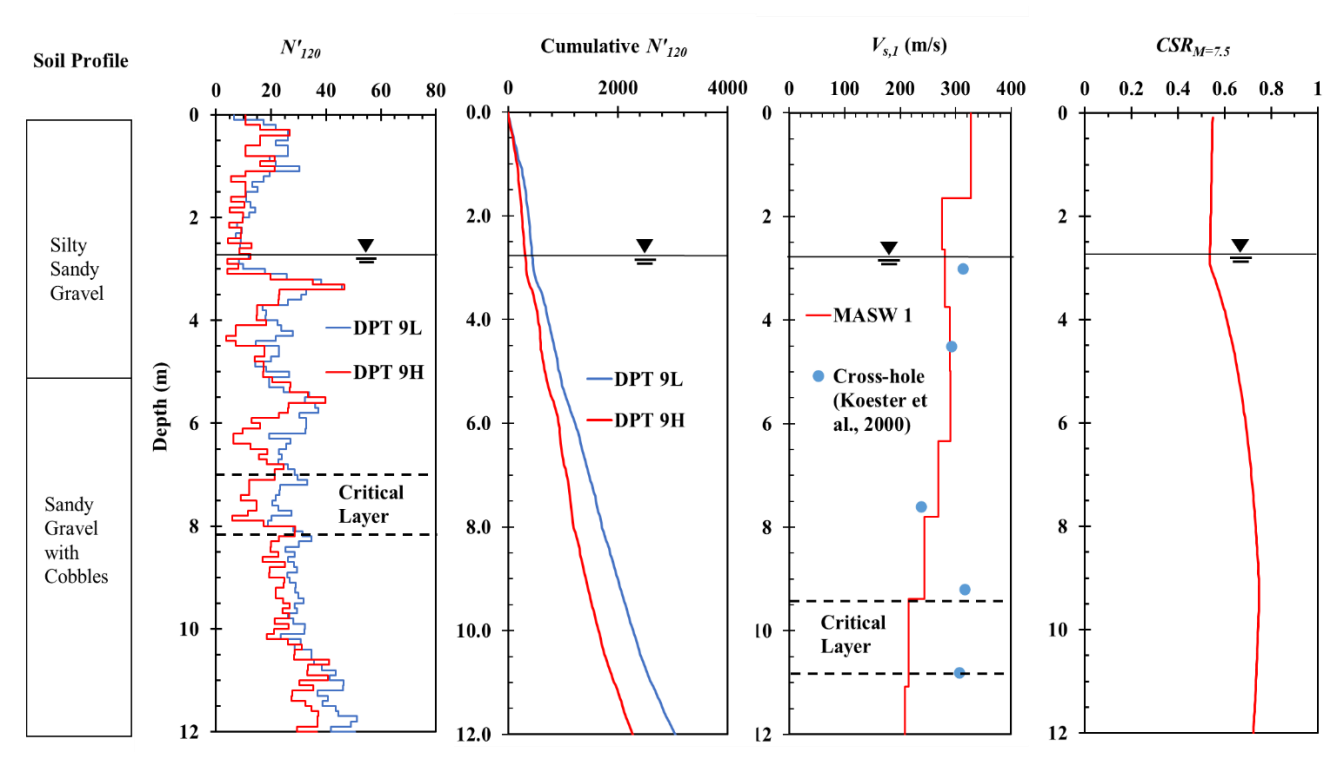


Fig. 13. Profile of soil strata, DPT N'_{120} and cumulative DPT N'_{120} for 63.5 kg (L) and 154 kg (H) hammer, $V_{s,1}$ and $CSR_{M=7.5}$ for Site 9 at Seward.

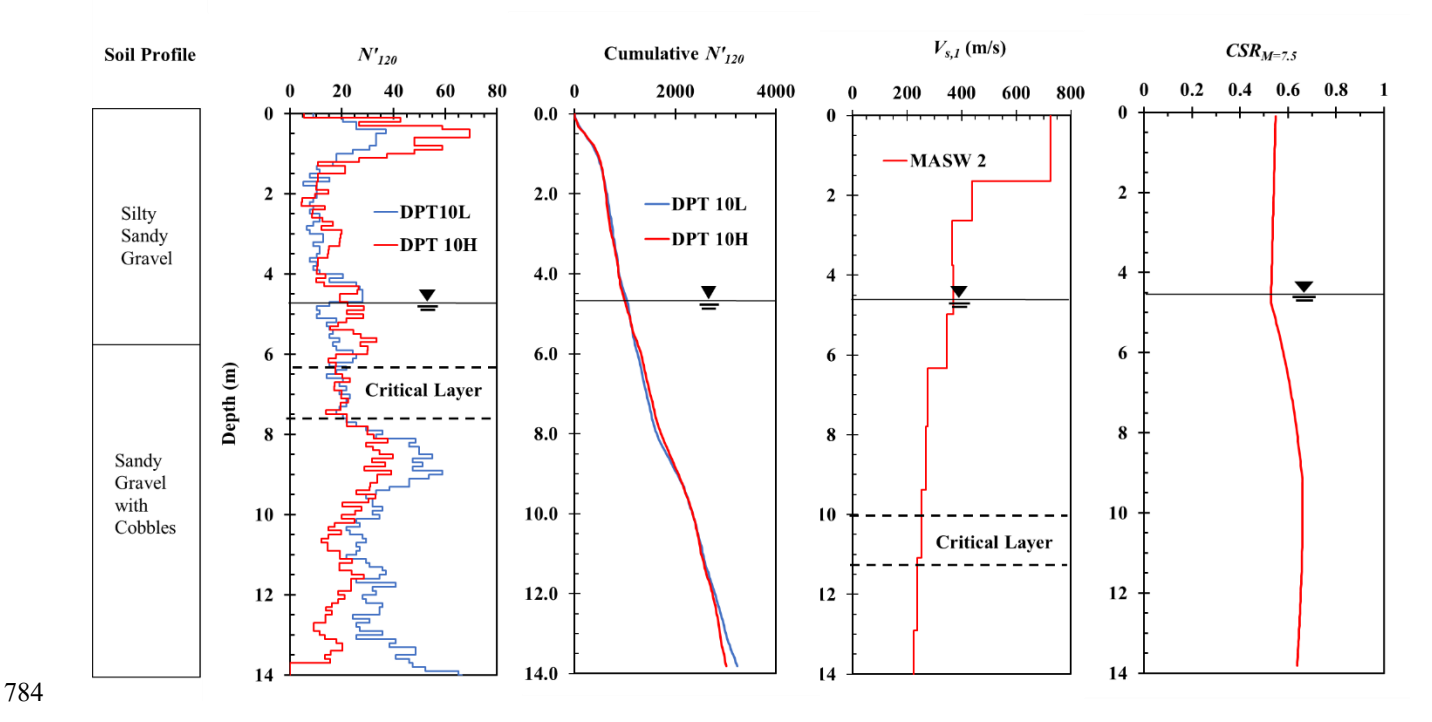


Fig. 14. Profile of soil strata, DPT N'_{120} and cummulative DPT N'_{120} for 63.5 kg (L) and 154 kg (H) hammer, $V_{s,1}$ and $CSR_{M=7.5}$ for Site 10 at Seward.

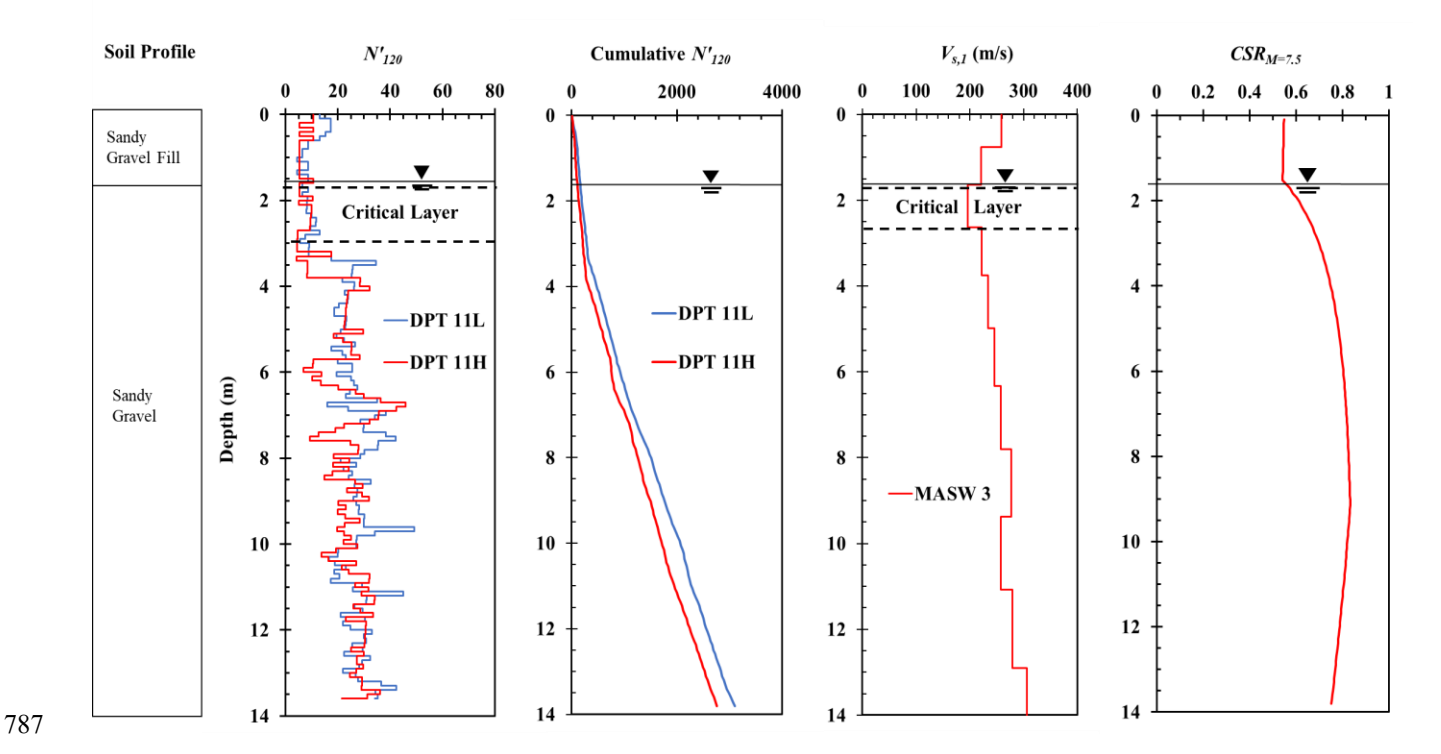


Fig. 15. Profile of soil strata, DPT N'_{120} and cummulative DPT N'_{120} for 63.5 kg (L) and 154 kg (H) hammer, $V_{s,1}$ and $CSR_{M=7.5}$ for Site 11 at Seward.

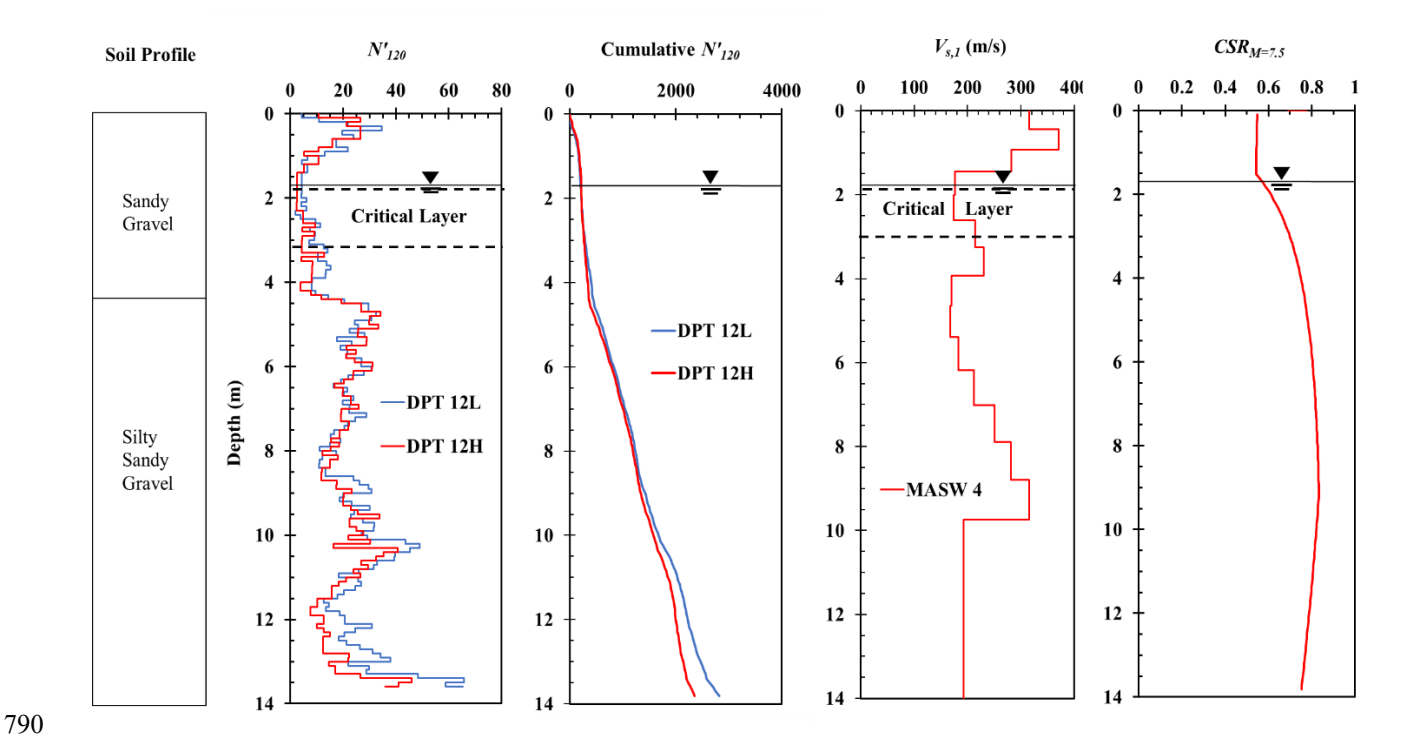


Fig. 16. Profile of soil strata, DPT N'_{120} and cummulative DPT N'_{120} for 63.5 kg (L) and 154 kg (H) hammer, $V_{s,1}$ and $CSR_{M=7.5}$ for Site 12 at Seward.

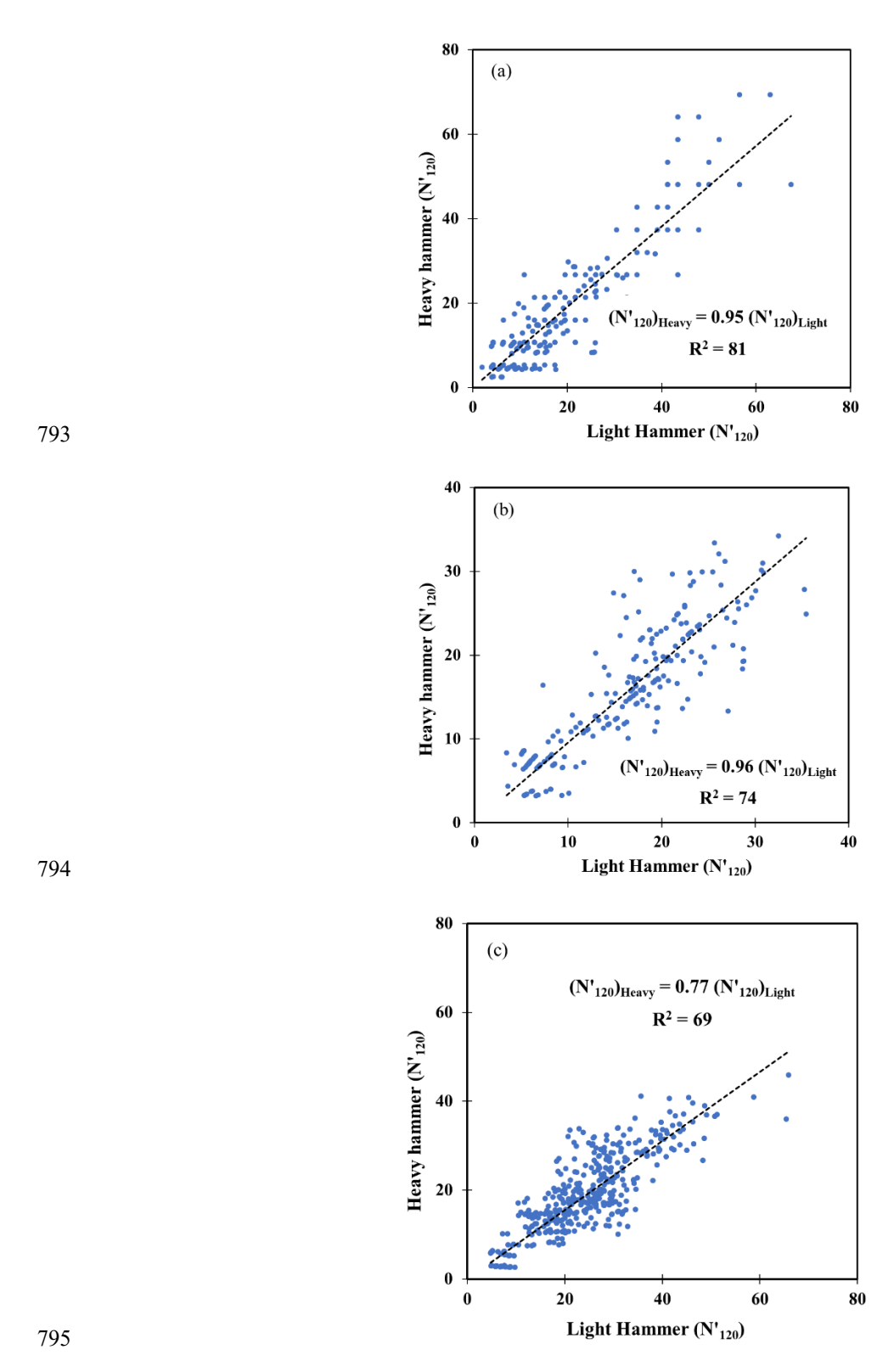


Fig. 17. Comparison of DPT N'_{120} obtained from lighter hammer (63.5 kg) and the heavy hammer (154 kg) after energy correction (excluding Seward 9) for the depth of (a) 0-4 m, (b) 4-8 m and (c) beyond 8 m.

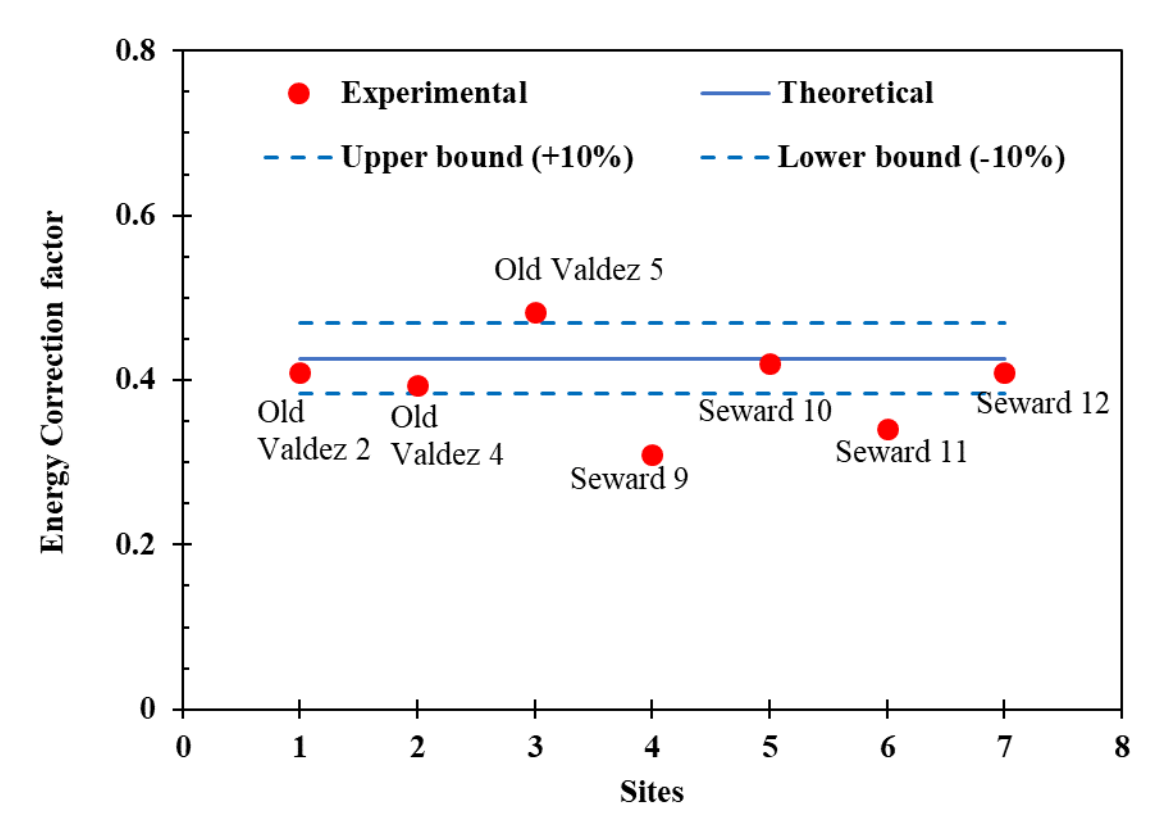


Fig. 18. Comparison between theoretical and experimental energy correction factors for sites at Seward and Old Valdez.

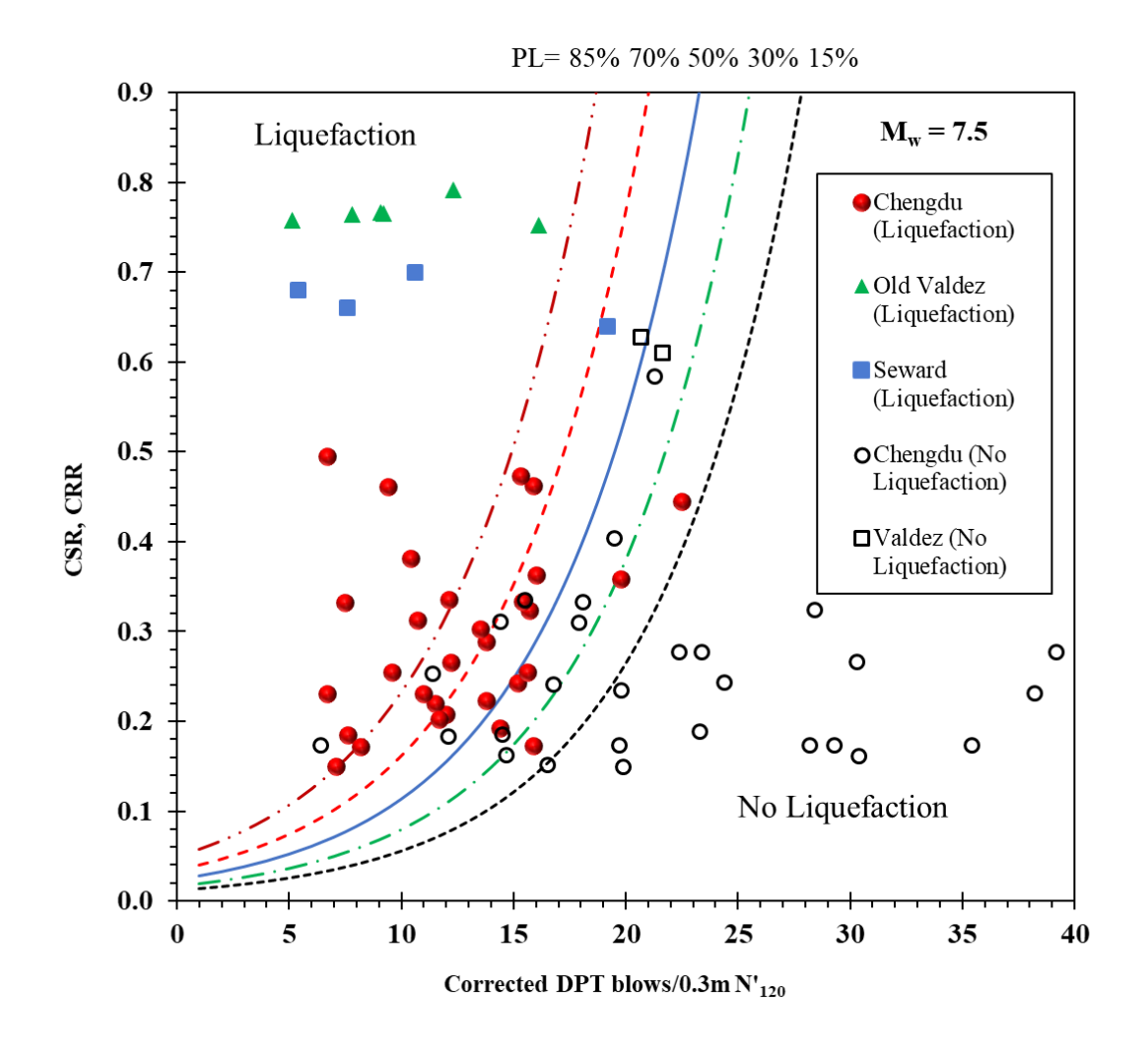


Fig. 19. Evaluation of liquefaction potential of Valdez and Seward sites with respect liquefaction triggering curves based on the Chinese DPT for gravelly soil (Cao et al. 2013)

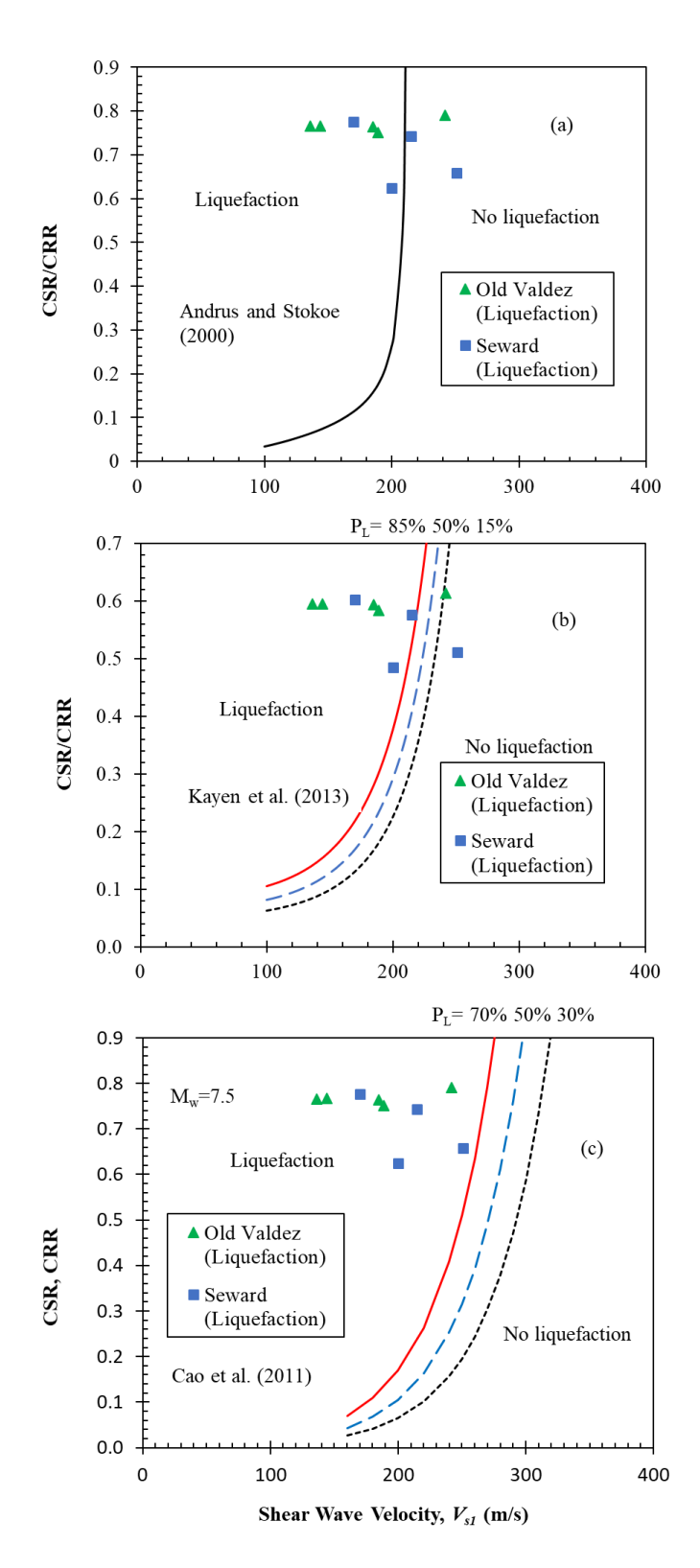


Fig. 20. Evaluation of liquefaction potential of Valdez and Seward sites with respect to $V_{s,l}$ -based liquefaction triggering curves given by (a) Andrus and Stokoe (2000) and (b) Kayen et al. (2013) for sand and (c) Cao et al. (2011) for gravels.